Caspian Sea levels over the last 2200 years, with new data from the S-E corner

Suzanne A.G. Leroy, Paula J. Reimer, Hamid A. K. Lahijani, Abdolmajid Naderi Beni, Eberhard Sauer, Françoise Chalié, Klaus Arpe, François Demory, Kenneth N Mertens, Dahvya Belkacem, et al.

Caspian Sea levels over the last 2200 years, with new data from the S-E corner

S.A.G. Leroy [a,b,*], P.J. Reimer [c], H.K. Lahijani [d], A. Naderi Beni [d], E. Sauer [e], F. Chalié [f], K. Arpe [g,1], F. Demory [f], K. Mertens [h], D. Belkacem [i], A.A. Kakroodi [j], H. Omrani Rekavandi [k], J. Nokandeh [l], A. Amini [m]

[a] *Aix Marseille Univ, CNRS, Minist Culture, LAMPEA, UMR 7269, 5 rue du Château de l'Horloge, 13094 Aix-en-Provence, France*
[b] *School of Environmental Sciences, University of Liverpool, L69 3GP Liverpool, UK*
[c] *14CHRONO Centre for Climate, the Environment and Chronology, Queen's University Belfast, Belfast BT7 1NN, UK*
[d] *Iranian National Institute for Oceanography and Atmospheric Science (INIOAS), No.3, Etemadzadeh Street, West Fatemi Avenue, Tehran, Iran*
[e] *School of History, Classics and Archaeology, University of Edinburgh, UK*
[f] *Aix Marseille Univ, CNRS, IRD, INRAE, CEREGE, Aix-en-Provence, France*
[g] *Max Planck Institute for Meteorology, Hamburg, Germany*
[h] *Ifremer, LITTORAL, Concarneau, France*
[i] *Institut Méditerranéen de Biodiversité et d'Ecologie Marine et Continentale (IMBE), Aix Marseille Univ, Avignon Université, CNRS, IRD, IMBE, Aix-en-Provence, France, Technopôle de l'Environnement Arbois-Méditerranée, BP 80, 13545 Aix-en-Provence Cedex 4, France*
[j] *Faculty of Geography, Department of Remote Sensing and GIS, University of Tehran, Iran*
[k] *Great Gorgan Wall Cultural Heritage Base, Iranian Cultural Heritage, Handicrafts and Tourism Organization, Gorgan, Iran*
[l] *National Museum of Iran, Research Institute of Cultural Heritage and Tourism, Tehran 113665-4364, Iran*
[m] *Department of Geology, Faculty of Sciences, Golestan University, P.O. Box 155, Gorgan 49138-15759, Iran*

A B S T R A C T

A revision of the data used to build the Caspian Sea level curve over the last 2200 years BP has been made based on a combination of geological and archaeo-historical data, using only those for which sufficient metadata were available. This compilation is completed by new sedimentological and palynological data from the south-east corner of the Caspian Sea, especially close to the known termini of the Sasanian Gorgan and Tammisheh Walls. A new calibration of the radiocarbon dates was used, i.e. with a freshwater offset reservoir of 351 ± 33 years. A literature survey of the Derbent lowstand indicated that this term has different definitions, depending on authors; it is thus to be used with caution. Here we therefore prefer to distinguish the mid-Sasanian lowstand and the later Medieval moderate lowstand. The "2600 years BP highstand" has not been found, mostly due to the calibration or recalibration of the datapoints used; data are indeed lacking at that time. Instead, a younger Parthian highstand (around 50 BC–50 AD) is clearly defined. The maximal amplitude and speed of change of the Caspian Sea level were respectively of >15 m and 14 cm per year. Compared to last century, the latter rate is 25% higher, but the amplitude is more than five times larger. The climatic causes of the Caspian Sea level changes are discussed. It is far from a simple case of temperature forcing; temperature forcing may result in several effects, that may impact the Caspian Sea level variations in opposite ways. Moreover, human intervention on river diversion and natural hazards were likely, for several time periods.

1. Introduction

The coastal zones are the most densely populated regions of the world. It is thus of crucial importance to understand how and why water levels are changing, not only along marine coasts, but also along the shores of large lakes. The Caspian Sea is the largest inland body worldwide. Its south and south-western coasts have the largest urban concentrations with several towns of >800,000 inhabitants (Kurtubadze, 2020). In the last century, the water levels of the Caspian Sea have changed dramatically at a scale close to 3 m, with direct impact on

oil and gas infrastructure as well as agricultural and urban development along the coast (Fig. 1a, b and c) (e.g. Kakroodi et al., 2014a).

The Caspian Sea levels (CSL) are mostly dependent on the main inflowing river, i.e. the Volga River whose drainage basin is in middle and northern Europe (Leroy et al., 2020). It brings, depending on the year, between 80 and 90% of the water. The Volga discharge on its own thus explains a large portion of the CSL variability (Arpe and Leroy, 2007). Over time, further prominent factors are evaporation and wind direction (Arpe et al., 2020), and the presence of other important inflowing rivers such as the Amu Darya and human intervention (Naderi Beni et al., 2013; Haghani et al., 2016; Leroy et al., 2019a, 2020; Sala, 2019) (Fig. 1). Natural hazards and human activities have repeatedly modified the course of the Amu Darya and Syr Darya in their deltas near the Aral Sea, causing several river diversions from the Aral Sea to the Caspian Sea leading to rather sudden CSL rises and falls in the last 2500 years (Sala, 2019) (Fig. 1a).

Over the last millennium, the levels may have changed by >9 m, perhaps even by as much as 19 m (Naderi Beni et al., 2013). Over the Late Pleistocene-Holocene period, CSL amplitude reached more than 100 m (Svitoch, 2012; Maksaev et al., 2015; Bezrodnykh and Sorokin, 2016). It has recently been shown that, via an impact on the width of the coastal plain at the foot of the Alborz Mountains (Fig. 1), the CSL have had a direct impact on the diet of Mesolithic and Neolithic populations (Leroy et al., 2019b). When sea levels were high, seal, deer and water bird bones were found in coastal caves, whereas when sea levels were low, the coastal plain significantly enlarged providing hunters with access to a wide range of herbivores (Leroy et al., 2019b). From a geomorphological point of view, fluctuations of river base levels have been shown to modify river courses and river downcutting far inland (>400 km in the Kura Basin) (Ollivier et al., 2016) (Fig. 1b). Avulsions of Caspian rivers have taken place repeatedly, lagoons have appeared and disappeared, often driven by CSL changes (Hoogendoorn et al., 2005; Kroonenberg et al., 2007; Leroy et al., 2011; Haghani and Leroy, 2016).

These changes in the level and the size of the Caspian Sea have had an influence not only on the regional climate but also, by teleconnections, worldwide (Arpe et al., 2019; Koriche et al., 2021); hence the importance to understand CSL drivers in order to better prepare mitigation plans.

Fig. 1. Maps
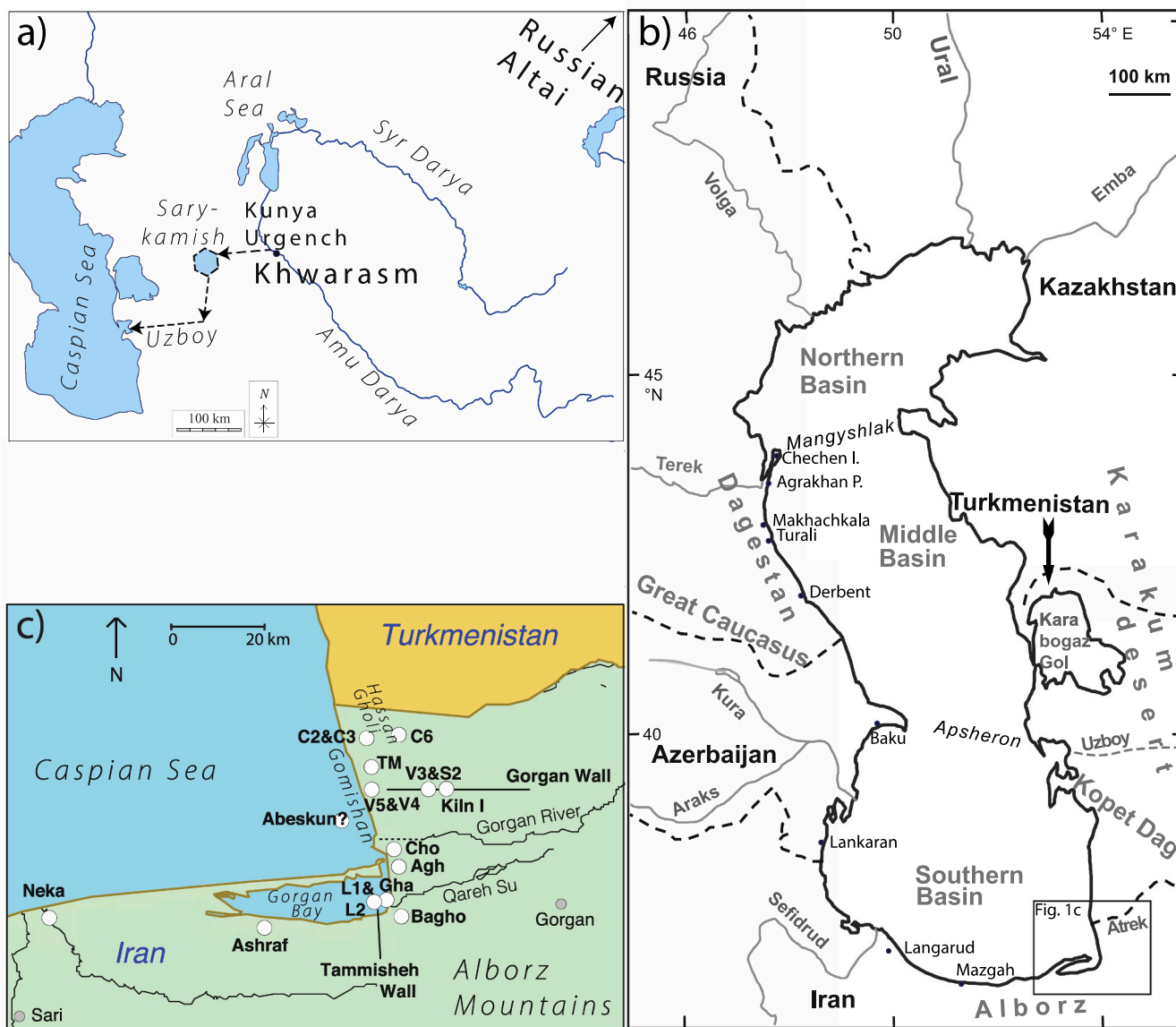**a:** The Caspian Sea with its link to the Amu Darya (black arrow).**b:** The Caspian Sea with the main data points around the sea.
c: Details of the points used for the S-E corner of the CS (white circles). Small grey circles for towns.

Despite over a century of research, the CSL curve is still poorly known even for the last millennia (Leroy et al., 2020). The methods used for the reconstructions in these recent times often combine radiocarbon dating of geological sequences with archaeological and historical information. Unfortunately, the CSL curves of Varushchenko et al. (1987), Karpychev (2001), Hoogendoorn et al. (2010) and Svitoch (2012), are not only different but often contradictory. Fig. 6 in Naderi Beni et al. (2013) publication illustrates well this difficulty for the last millennium with data from Brückner (1890), Varushchenko et al. (1987) and Karpychev (1998, 2001) displaying overlapping and criss-crossing curves.

Metadata are often incomplete or even absent, such as radiocarbon dates in Svitoch (2012), in the Volga Delta study of Hoogendoorn et al. (2010) and the various sites of Rychagov (1977). When some metadata for each point on the curve are available, such as in Varushchenko et al. (1987) and Karpychev (1993, 2001) allowing adjusting CSL curves with a new radiocarbon calibration, it remains nevertheless hard to obtain a meaningful synthesis, as essential information such as either elevation or coordinates are not available. These problems highlight the need of providing clear metadata and to calibrate – and recalibrate when progress is made – radiocarbon dates to combine these with the usually more precise archaeological and historical data. Without this, the combination of calendar and non-calendar dates is misleading. Difficulties occur in integrating old (sometimes with large standard deviations) and more recent datasets. Moreover, calibration of the Caspian Sea radiocarbon dates has been so far more difficult than calibration of dates from the sea or lakes due to its fluctuating state between sea and lake over geological times (Hoyle et al., 2021). This is de facto slowing down relative sea-level reconstructions such as those already made in the Mediterranean Sea combining geology and archaeology (e.g. Marriner and Morhange, 2006).

The well-cited CSL curve of Rychagov (1997) is lacking data points between approx. 2600 and 800 years ago, i.e. a gap of ca 1800 years shown by a dashed line. This is only partially filled by the compilation by Naderi Beni et al. (2013) with a starting point at ca 1000 yr ago. This period without data is of great interest to archaeologists and historians, especially for the regions inhabited in the past around the Caspian Sea, i. e. in general the south, south-west and south-east coasts. An outstanding feature are the long walls built to defend the Persian empire's inhabitants from northerners in the Late Sasanian era (5th–6th century AD) (Kudrjavcev and Gadžiev, 2002; Aliev et al., 2006; Sauer et al., 2013), with several walls reaching the Caspian Sea. Most of them were built between the Caspian coastline and a relief, such as the Alborz or Caucasus Mountains when the sea level was lower than at present (Fig. 1b and c).

A compilation of data including new information is presented here with the aims of:

1. Reconstructing palaeoenvironments (mostly by pollen and dinocysts analyses) and CSL at the end sections of the Gorgan and Tammisheh Walls, built during a period of lowstand in the Sasanian era, an era spanning from 224 AD to 651 (Sections 3.1, 3.2 and 3.3), including the Gorgan Wall project and other previous ones in the region.
2. Filling in the sea level curve gap between the published "2600 yr BP highstand" and the CSL curve covering the last 1000 years, compiling geological (Sections 3.4 and 3.5) and archaeo-historical data (part 2).
3. Finally, discussing a more complete sea level curve for the last 2200 years based on the combination of geological and archaeo-historical data and searching for water level drivers (part 3).

Additionally, the recent release of the new calibration curve IntCal20 (Reimer et al., 2020) and the use of a new freshwater reservoir offset correction lends to an in-depth reassessment of published and unpublished radiocarbon dates (Stuiver et al., 2021) with the possibility to either recalibrate them or, even for some, to calibrate them for the first time.

1.1. Setting

The Caspian Sea is a large lake (386,400 km^2 in 2017), located between geographical Europe and south-western Asia (Fig. 1a). It is divided in three sub-basins (Leroy et al., 2020). The northern one has a maximal depth of 25 m, the middle one 788 m, and the southern one 1025 m. Its drainage basin (~3,500,000 km^2 with its eastern drainage) extends between 36 and 62° latitude North. The water salinity is close to 13 psu in the south and middle basins, whereas it decreases to nearly zero in the northern basin, especially close to the large Volga and Ural river mouths. Due to the latitudinal extension of the water body, it is surrounded by various climates from subtropical humid in the south to desertic in the east and north and becoming temperate in the northern part of its drainage basin (Leroy et al., 2020).

The focus area under investigation is along the SE coast of the Caspian Sea (Fig. 1c). The south coast is rather narrow as it abuts the Alborz mountains with its diverse Hyrcanian forest. On the contrary, on the east coast, is the fairly large Gorgan Plain that extends from the Alborz Mountains to the Karakum Desert (Fig. 1b and c). It is used for agriculture, especially rice, wheat, barley and cotton. In the south-east corner lies the shallow Gorgan Bay, that is a semi-closed lagoon protected from the Caspian Sea by a spit, the Miankaleh Spit. The sea is very shallow not only in the bay but also in the whole of the SE Caspian Sea, making the whole area sensitive to vertical changes as it translates into large horizontal changes. A palaeo-delta was found at the eastern end of the spit that closes the bay, where the current main outflow of the bay is located (Kakroodi et al., 2014b). The former Hassan Gholi (Esenguli or Lagoon of Hassan) in the north of the Gorgan Plain straddles the border between Iran and Turkmenistan (Fig. 1c). It is separated from the Caspian Sea by a sill that protects it from the sea (Kakroodi et al., 2012; Naderi Beni et al., 2014), and is fed by the Atrek River from the north and by seasonal rivers from the east. The elevation of eastern parts of the lagoon is around 28 m below mean sea level (m bsl) and thus currently at the same level than the CS. However today this lagoon is almost dry due to the superimposition of human intervention and upstream over-exploitation of water over fluctuating CSL (Kakroodi et al., 2012).

The region is known for ancient Palaeolithic, Mesolithic and Neolithic human occupations (Leroy et al., 2019b) and for its many archaeological and historical sites. The development and collapse of some of the settlements may clearly be linked to CSL changes. Of the several Sasanian Walls, at least three carry on under water, as they were built at a time when the CSL was lower. Other towns and harbours appeared and disappeared as the coastline changed throughout the centuries. Because of the economical and demographical importance of the region, several ancient writers have recorded these changes (e.g. in Naderi Beni et al., 2013).

2. Material and methods

2.1. Elevations

Elevations are given in metres below sea level with regards to the Baltic 1977 datum at the Kronstadt tide gauge (Kouraev et al., 2011). The Caspian Sea was at a − 27.45 m on 10 October 2016 when the GW16 cores were obtained as part of the Gorgan Wall project (Hydroweb, 2021). In 2021, it had already fallen below −28 m following a trend that started in 1995. Elevations for geological data used here are usually minimal water level elevations as they indicate the elevation of the water-sediment interphase and not the elevation of the water surface that is higher. Archaeo-historical informations usually indicate a maximal water level.

2.2. Sites

The Gha core was taken at the SE corner of the Gorgan Bay near the village of Gharasoo (Leroy et al., 2019b) (Fig. 1c). The GW16V4 (N 37°

7′ 25.98, E 54° 03′ 24.72) and GW16V5 cores (for short V4 and V5) were taken between the coast and the surmised western terminus of the Gorgan Wall (Leroy et al., 2022) (Fig. 1c). The GW16V3 core (for short V3) was taken on a small ditch close to the Sasanian kiln I along the Gorgan Wall (Leroy et al., 2022). The TM core was obtained from a small elevation at the SE corner of the Hassan Gholi, Gomishan district (Leroy et al., 2013a; Kakroodi et al., 2015; Fig. 1c). All these sites were chosen as they contain sediment deposited along the coast of the Caspian Sea or in lagoons, under varying water depths.

2.3. New and old sequences

New analyses were made on four of these five cores. For the top of the **Gha** core in Gharasoo (Fig. 1c), the lithology was provided in Leroy et al. (2019b), while palynology (pollen and dinocysts) is presented here for the first time. The lithological description and magnetic susceptibility of core **V4** are new data. Details of the lithology and the magnetic susceptibility measurements for core **V5** (west of Gorgan Wall's westernmost point detected to date; Fig. 1c) may be found in Leroy et al. (2022) where the curves of only a couple of pollen and dinocyst taxa were included. For the current publication, further palynological work was thus applied to this core, i.e. increased sampling resolution and first presentation of the full spectra. Additionally, the top of the nearby **TM** core (Leroy et al., 2013a) is used for comparison (Fig. 1c). While the pollen spectra of this core remain those already published, it was necessary to provide new dinocyst data for preparing a diagram fit for comparison, by increasing the sums of the dinocyst spectra.

2.4. Magnetic susceptibility and palynology methods

For the new data presented in this publication, the following methods were used. For magnetic susceptibility (MS) measurements of the GW16 cores, a Bartington MS2 susceptibilimetre was used with a MS2E surface probe at 2 cm resolution directly on the freshly split core surface.

The palynological sample volume was between 1 and 2.5 ml. Initial processing of samples involved the addition of sodium pyrophosphate to deflocculate the sediment. Samples were then treated with cold hydrochloric acid (10%) and cold hydrofluoric acid (32% or for some 58–62%), then hydrochloric acid again. The residual fraction was screened through 125 (or 200 μm) and 10 μm mesh sieves. Final residues were mounted on slides in glycerol and sealed with varnish. *Lycopodium* tablets were added at the beginning of the process for concentration estimation in number of pollen and spores per ml of wet sediment (without non-pollen palynomorphs or NPP).

The taxonomy and the ecological preferences of the Caspian dinocysts have been detailed in Mudie et al. (2017) and in Leroy et al. (2018). An additional form with a morphology between *Galeacysta etrusca* and *Spiniferites cruciformis* A was found. The diagrams were plotted using psimpoll with a 10× exaggeration curves and black dots for values lower than 0.5% (Bennett, 2007). In the pollen diagram, the spores, the aquatic pollen and the NPP and in the dinocyst diagram, the foraminifera, are expressed in percentages of the terrestrial pollen and dinocyst sums respectively.

Lingulodinium machaerophorum process lengths were measured in core TM following the method described in Mertens et al. (2012). All measurements were made using a Zeiss Axioskop 2 equipped with an AxioCam MRc5 digital camera (Axiovision v. 4.6 software) and 100× objective. For each sample, the average of the length of the three longest visible processes and the largest body diameter of 30 cysts per sample were measured, when possible. Measuring 30 cysts yields reproducible results (Mertens et al., 2009); average process length per sample for L. *machaerophorum* is reproducible within ~1 μm. The length of each process was measured from the middle of the process base to the process tip. It is important to note that no cysts without processes (i.e. "zero" process length) were included in the analysis, because of the difficulty of

species identification associated with these forms and the desire to exclude observer bias from the measurements. For each cyst, three processes could always be found within the focal plane of the light microscope. Fragments representing less than half of a cyst and cysts with mostly broken processes were not measured. The use of the equation $SSS_{summer} = 0.026*PL^2 - 0.0145*PL + 12.136$ ($R^2 = 0.91$) of Mertens et al. (2012) allows reconstructing average summer salinity at the sea surface.

Twenty-three samples (two of them barren) in core Gha and 39 samples (13 barren) in core V5 were treated for palynology. The average terrestrial pollen sum is 343 (in between 283 and 483) for the Gha sequence and 329 (in between 110 and 567) for the V5 sequence. The average dinocyst sum is 339 (in between 84 and 1561) for the Gha sequence and 488 (in between 29 and 1302) for the V5 sequence. The dinocyst sums of the TM core was increased to a minimum of 80.

2.5. Water level indicators

Estimation of palaeowater depths is derived from a range of combined sedimentological and palynological observations. Firstly, we used fairly basic sedimentological indicators. A fine-grained sediment is mostly deposited in a deeper and quieter environment than a sandy one. Oxydised sediment is usually considered as formed in high energy waters, thus shallower water than grey one. Hiati are clear signs of erosion and low water levels (outside human intervention). High magnetic susceptibility values show detrital input and thus often high energy aquatic environments. Broken shell layers are often due to wave action, thus formed at shallow water depth.

Secondly palynological indicators are diverse. For example, the presence of fern and moss spores, *Concentricystes* (NPP) and high reworked palynomorph percentages are reflecting river input. The dinocyst *Lingulodinium machaerophorum* may reflect warm and/or nutrient rich waters. The P/D ratio is the ratio of the concentration of pollen on that of dinocysts (McCarthy and Mudie, 1998). When it is high the environment is more continental than when it is low. Absence of palynomorphs is usually due to *syn-* or post-deposition oxidation. Only a selection of water-level indicators is shown in the three palynological diagrams (full diagrams are provided in SI).

2.6. Radiocarbon calibration

Since the Caspian Sea is not part of the global ocean, for calibration of radiocarbon ages, it is more appropriate to use an atmospheric calibration curve with a correction for the 'freshwater' reservoir offset (FRO) rather than the marine calibration curve with a ΔR value, as previously done (e.g. Leroy et al., 2007, 2011, 2019a and b). The FRO for the Caspian Sea is not straightforward given the large size and depth of the water body; but it may be approximated by using known age shells and paired lacustrine/terrestrial samples.

For known age samples (e.g. from museum collections), the FRO is calculated from the difference between the measured shell/organism age and the atmospheric age taken from the calibration curve. However for terrestrial samples collected since 1850 AD, we have to correct for the ^{14}C decline in the atmosphere due to fossil fuel CO_2 input. We estimate the fossil fuel correction from the difference in a production-driven model and the measured tree-ring [14]C (Stuiver and Quay, 1981). But instead of using a simple exponential increase in the contribution of fossil fuel to the atmosphere from the endpoints, we use the Stuiver-Quay model with a correction of 0 ^{14}C yr for 1860 AD increasing to 126 ^{14}C yr by 1950 AD with an uncertainty of 16 ^{14}C yr. We use measured ^{14}C values of shells and a seal bone published by Kuzmin et al. (2007) and Olsson (1980) (Table 1). One sample collected in 1953 has a much lower FRO than the other samples, especially after correcting for fossil fuel. It is possible that this sample included ^{14}C from nuclear weapons testing and so was not used in the weighted mean FRO.

Two paired lacustrine/terrestrial samples – a charcoal and shell pair

Table 1
Radiocarbon ages from museum collections and their freshwater reservoir offsets.

Collection year	^{14}C BP	Reservoir Age (^{14}C yr)	Ffcorr (^{14}C yr)	FRO corr (^{14}C yr)	Genus	Species	Locality	Reference
Caspian Sea 'freshwater reservoir offset'								
1953	410 ± 40	205 ± 41	−138	67 ± 44	*Didacna*	*crassa*	Garabogaz_Spit	Kuzmin, 2007
1899	455 ± 50	358 ± 50	−26	332 ± 52	*Phoca*	*caspica*	Kulalai, Caspian Sea	Olsson, 1980
1900	465 ± 35	359 ± 31	−27	332 ± 35	*Didacna*	*trigonoides*	Cheleken_Peninsula	Kuzmin, 2007
1900	570 ± 30	369 ± 36	−27	342 ± 39	*Didacna*	*trigonoides*	Chechen_Island	Kuzmin, 2007
1920	455 ± 30	433 ± 31	−50	383 ± 35	*Didacna*	*trigonoides*	Sulak_River_Mouth	Kuzmin, 2007
			wt. mean	304				
			std. dev.	120				
Without sample collected in 1953								
1899	455 ± 50	358 ± 50	−26	332 ± 52	*Phoca*	*caspica*	Kulalai, Caspian Sea	Olsson, 1980
1900	465 ± 35	359 ± 31	−27	332 ± 35	*Didacna*	*trigonoides*	Cheleken_Peninsula	Kuzmin, 2007
1900	570 ± 30	369 ± 36	−27	342 ± 39	*Didacna*	*trigonoides*	Chechen_Island	Kuzmin, 2007
1920	455 ± 30	433 ± 31	−50	383 ± 35	*Didacna*	*trigonoides*	Sulak_River_Mouth	Kuzmin, 2007
			wt. mean	350				
			std. dev.	26				

from a trench at site S2 (Leroy et al., 2022) and a peat and shell pair from the Agrakhan sand bar are available (Karpychev, 2001) (Fig. 1b and c; Table 2). The FRO for the paired material is calculated from the difference between the measured radiocarbon age of the lacustrine sample and the terrestrial sample. The pair from site S2 resulted in an FRO of only 6 ± 40 ^{14}C yr. It is likely that there is either an 'old wood' effect giving the charcoal an apparent older age or that the pair are not really contemporaneous. The S2 pair was thus omitted. The weighted mean of all the accepted samples thus gives a FRO of 351 ± 33 ^{14}C yr (Table 3). This FRO value was used to correct the measured radiocarbon ages before calibration for all the samples with IntCal20 (Reimer et al., 2020). It is noteworthy that the new FRO calibration is actually not far from a calibration with a marine correction that is usually 400 ^{14}C years for the last millennia (Heaton et al., 2020).

Forty-one dates were thus collected and calibrated. Most were made on shells, with the exception of one bulk sediment and five on selected organic material such as charcoal, leaves or woody rootlets. To distinguish calibrated radiocarbon dates from uncalibrated radiocarbon dates and historical dates, the former are indicated as cal BC or cal AD while uncalibrated radiocarbon dates are given as BP and historical dates as BC or AD.

3. Part 1: new geological data and compilation

In order to increase the number of sequences addressing the question of CSL over the last 2200 years, the results of four sequences in the S-E corner of the Caspian Sea are presented for the first time and/or have been updated: i.e. cores Gha, V4, V5 and TM (parts 1.1, 1.2 and 1.3).

Then, geological data with radiocarbon dating from the S-E corner of the Caspian Sea are compiled (part 1.4), as well as from other parts around the Caspian Sea (part 1.4). In part 1.5, some general trends in highstand and lowstand are proposed based on these dates over the last 2200 years.

3.1. Gorgan Bay: top of the Gharasoo sequence

The details of the lithology of the top of the Gha core were published in Leroy et al. (2019b) without palynological data and with only two out of the three radiocarbon dates that are now available. In brief, above a sandy silt layer horizon (336–318 cm depth) interpreted as a hiatus, a

Table 2
Radiocarbon ages from terrestrial/marine pairs and their freshwater reservoir offsets.

	terrestrial ^{14}C BP	shell ^{14}C BP	FRO (^{14}C yr)
Leroy S2	959 ± 28	965 ± 28	6 ± 40
Karpychev	1400 ± 120	1850 ± 140	450 ± 184

Table 3
Weighted means of all freshwater reservoir offsets and without the S2 pair.

All		Without S2 charcoal/shell pair	
Location or reference	FRO (^{14}C yr)	Location or reference	FRO (^{14}C yr)
Kulalai, Caspian Sea	332±52	Kulalai, Caspian Sea	332±52
Cheleken_Peninsula	332±35	Cheleken_Peninsula	332±35
Chechen_Island	342±39	Chechen_Island	342±39
Sulak_River_Mouth	383±35	Sulak_River_Mouth	383±35
S2 charcoal/shell	6±40		
Karpychev peat/shell	450±184	Karpychev peat/shell	450±184
wt. mean	285	wt. mean	351
std. dev	153	std. dev.	33

clayey silt sediment occurs until sharp change at 185 cm depth, where a massive dark olive clayey silt occurs (Fig. 2). From another sharp change at 155 cm, the sand fraction increases until the top. The sediment is generally brown except for the lower sandy silt (336–318 cm) and the clayey silt at 230–200 and 185–160 cm that are olive grey. Three radiocarbon dates were obtained on shells at 310, 199 and 152 cm depth, with a median probability of 1550 cal BC, cal 170 AD and finally cal 1550 CE respectively (Table 4a).

Pollen zone GhP-8 (336–178 cm): The arboreal pollen (AP) % are high with a strong occurrence of *Alnus, Quercus, Parrotia persica, Pterocarya, Juglans, Ulmus-Zelkova* and *Vitis* (Fig. 3 and SI 1). Amaranthaceae reach a minimum at 12%, while *Artemisia* are as low as 5%, before a small increase at the end of this zone. *Polygonum aviculare-bistorta*-t. is frequent. Monolete psilate spores increase in the middle of this zone, while trilete psilate spores are continuously present. *Concentricystes* and *Azolla-Salvinia* remains (massulae and microspores) are nearly continuously present. Pollen zone GhP-9 (178–94 cm): In comparison to the preceding zone, AP values drop significantly, especially *Alnus* and *Pterocarya*. *Artemisia* reaches a minimum. Amaranthaceae and Liguliflorae increase. The fern spores increase, and reworked elements are high. Fungal spores are very high. *Concentricystes* is still regularly present.

Dinocyst zone GhD-8 (336–153 cm) (Fig. 3 and SI 2): The assemblages show dominant and increasing values of *Impagidinium caspienense*. *Lingulodinium machaerophorum* are abundant. *Spiniferites cruciformis* and *Brigantedinium* sp. are frequent. Occasional foraminifera are present. Concentration increases across this zone, despite some sharp fluctuations. Dinocyst zone GhD-9 (153–94 cm): *I. caspienense* values fall, while L. *machaerophorum* increases. *Brigantedinium* sp. are high in the last sample. Foraminifera are frequent.

The date at 310 cm depth (median probability of 1550 cal BC, or 3580–3440 cal BP) was obtained in a sample rich in L. *machaerophorum*
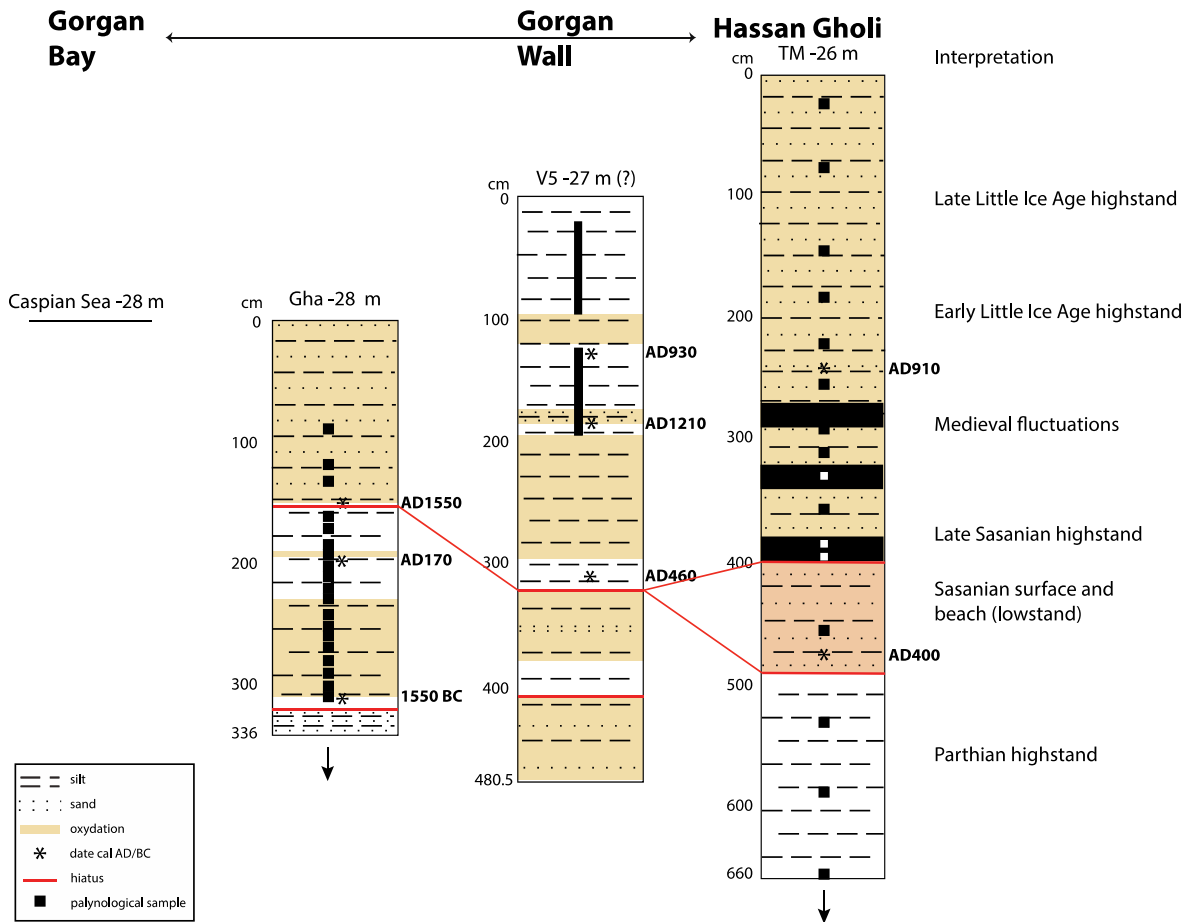
Fig. 2. Lithological logs of cores Gha, V5 and TM. The two downwards pointing arrows indicate that the cores are longer than plotted. Dates shown (*) are the cal AD/BC median probability of the radiocarbon calibrated age range.

and close to the sharp lithological change at 336–318 cm depth (Figs. 2, 3 and SI 1). One may question the validity of the date as this dinocyst has been shown to appear and develop in core TM only from a recalibrated date at 3250 cal BP (median probability) (Leroy et al., 2013b) (Fig. SI 7), thus it is difficult for this taxon to be present in an older sediment. It is however not impossible that the dated shells found on the hiatus belong to the sediment below the hiatus (and the occurrences of L. *machaerophorum* belong to the overlying sediment*)* (Leroy et al., 2013b).

The interpretation of the Gha sequence above 336 cm depth is as follows. The hiatus (336–318 cm) comes just after a sediment layer dated as 1550 BC or older. It is followed by a lagoonal facies. The forest of the Late Parthian period (an historical period from 247 BC to 224 AD, just before the Sasanian era), rich in trees from humid areas (*Pterocarya* and *Alnus*) is well recorded (zone GhP-8) with a clearly-marked human impact, demonstrated by the presence of *Juglans* (cultivated), *Vitis* (cultivated) and *Polygonum aviculare-bistorta-t.* (ruderal). The lagoon is widely connected to the open waters of the Caspian Sea in zone GhD-8. A strong continental influence is marked by river and erosional indicators (*Concentricystes*, psilate fern spores, reworked palynomorphs) (zones GhP-9a and GhD-9). Finally, the top of the sequence (barren in palynomorphs) ends with an oxidised, more sandy/silty and shell-rich unit, indicating a filling up of the lagoon in this location, which is now a wasteland, on the western edge of Gharasoo village, separated from the Caspian Sea by intermittent saltpans. The median probability of the calibrated age range of cal 1550 AD at 152 cm, just above the hiatus at 155 cm, indicates a lack of sediment for perhaps as much as 1400 years. Deposits of the Gorgan Bay (e.g. Bagho outcrop and others) usually contain a sediment attributed to the "2600 yr BP highstand" (see revised age below). To explain this absence, we need to invoke, beyond low

levels for part of the time, important management of the landscape during the Sasanian period. This has already been noted at the possible northern terminus of the Tammisheh Wall in cores GW16L1 and L2. Alternatively some erosion might have occurred due to the proximity to the thalweg of the Qareh Su (Gharasoo river) (Fig. 1) (Leroy et al., 2022).

3.2. Western terminus of the Gorgan Wall: Cores GW16V4 and GW16V5

The lithology of cores V4 (new) and V5 (adapted from Leroy et al., 2022) and radiocarbon dates (two published, one new) (Fig. 4) are provided below. Core V3A and B described and interpreted in Leroy et al. (2022) are shown in Fig. 4 for comparison). The cross-correlation between cores is based on visual sediment description (such as colour and grain size) and magnetic susceptibility values.

Core V4 is 370.5 cm long (Fig. 4). Very dark brown silty sand occurs from the base to 346.5 cm. It is followed, after a sharp change, by a grey silt until 308.5 cm, interrupted briefly by a brown silt horizon at 325.4–321.5 cm. Brown silt extends then from 308.5 to 148 cm. After a sharp change, a 6 cm layer of brown finely broken shell mash occurs. A greyish silt is deposited after another sharp change at 142 cm (only interrupted once by a brownish grey layer), and continues to the top. MS is 40 10^{-5} SI from 308.5 to ca 142 cm depth. It is low from 346.5 to 308.5 and from 148 to 142 cm. No radiocarbon dates were obtained. Core V5 is 480.5 cm long (Fig. 4). The lowermost part of this core, i.e. below 409 cm is a dark brown silty sand, as at the base of core V4. The lower part of core V5 (from 409 to 195 cm) consists of brown silt, except at 323.5–298.5 cm where the silt turns light olive grey. Sharp limits occur at 409 and 323.5 cm. Olive grey silt occurs from 195 to 184 cm,

Table 4

Geological data points used in this study with their elevation and radiocarbon dating and calibration information

a: in the SE corner of the Caspian Sea. MAR13 = Marine13; MAR09 = Marine09. * accuracy of 80 cm maximum, ** FRO: 351 ± 33, calib 8.20 showing only relative probability higher than 9% (rounded up), ^ On 2020 Google Earth map, first number distance to Caspian Sea, second number distance to lagoon, in bracket less relevant distance. ^^ rounded up. In blue and bold: sites from Hassan Gholi.

Absolute elevation top (m bsl)	Position	Distance from Caspian coast (km) ^	Site name	Type of sampling	Elevation of dated level (m bsl)	Core/trench depth (cm)	14C BP	IntCal20, 2 σ ** (cal AD/BC)	Median probability (cal AD/BC) ^^	Laboratory no	Dated material	Published information	Reference	Point number on Fig. 9
27.55	Gorgan Bay	0 (11.5)	L2A	core from water surface	28.1	58	1200 ± 29	1149–1274 AD (88%)	1200 AD	Poz-93,410	shell in grey silt	_	Leroy et al., 2022	8
					28.7	118	1735 ± 29	588–691 AD (89%) 741–773 AD (10%)	650 AD	Poz-93,411	shell in grey silt	_		7
27.35	Gorgan Bay	0 (11.5)	L1A	core from water surface	28.3	97	1855 ± 30	529–647 AD	570 AD	Poz-119,446	shell in grey silt	_	Leroy et al., 2022	6
					28.6	121	2440 ± 30	202 BC–20 AD	100 BC	Poz-119,447	shell in grey shell mash	_		2
27	S-E coast	0.8 (13.5)	Gha	core	28.5	152	705 ± 30	1456–1637 AD	1550 AD	Poz-132,910	shell at transition from dark olive grey mud to brown silt	_	unpublished	14
					29	199	2225 ± 30	59–249 AD	170 AD	Poz-38,787	shell in grey silty clays	279 BC (IntCal13). 121 AD. (MAR13)	Leroy et al., 2019a, b	
					30.1	310	3634 ± 25	1632–1489 BC	1550 BC	UBA-36126	shell in dark greyish brown silty mud after sand horizon	1996 BC (IntCal13) 1584 BC (MAR13)	Leroy et al., 2019a, b	
26.5?	Hassan Gholi	6.2 (2.8)	V5	core	27.8?	126	1465 ± 30	868–1022 AD	930 AD	Poz-132,909	shell at base of coarse silt layer rich in shell debris	_	unpublished	
					28.3?	184.5	1190 ± 30	1151–1278 AD	1210 AD	Poz-106,203	shell in brown sand	_	Leroy et al., 2022	
					29.6?	309.5	1980 ± 30	348–550 AD	460 AD	Poz-106,201	shell in grey silt	_	Leroy et al., 2022	
26.3*	east coast	7.9 (3.0)	C2	core	27.3	100	790 ± 30	1407–1522 AD (88%). 1576–1623 AD (13%)	1460 AD	Poz-51,060	shell in grey silt	1437–1681 AD (MAR09 deltaR 26 yr) 1440–1529 AD (60%) & 1543–1634 (40%) (IntCal09 RE 407 yr) 1433–1521 AD (86%) & 1591–1621 (34%) (IntCal09 RE 383 yr)	Naderi Beni et al., 2013	13
					31.9	562	2210 ± 30	70–253 AD	180 AD	Poz-51,061	shell in grey silt	59–239 AD (MAR09 deltaR 26 yr)	Naderi Beni et al., 2014	4
26.0*	Hassan Gholi	9.4 (5.2)	C3	core	27.45	145	665 ± 35	1460–1659 AD	1560 AD	Poz-51,062	shell in grey silt	1496–1872 AD (MAR09 deltaR 26 yr) 1490–1682 AD (80%) & 1737–1803 (20%) (IntCal09 RE 407 yr) 1486–1604 AD (68%) & 1607–1664 (32%) (IntCal09 RE 383 yr)	Naderi Beni et al., 2013	
					29.3	332	1875 ± 30	431–609 AD	550 AD	Poz-51,063	shell in grey silt	441–615 AD (MAR09 deltaR 26 yr)	Naderi Beni et al., 2014	
					30.45	445	2145 ± 30	153–378 AD	280 AD	Poz-51,064	shell in light brown shell layer	126–323 AD (MAR 09 DeltaR 26 yr)	Naderi Beni et al., 2014	

Table 4 (*continued*)

Absolute elevation top (m bsl)	Position	Distance from Caspian coast (km) ^	Site name	Type of sampling	Elevation of dated level (m bsl)	Core/ trench depth (cm)	^{14}C BP	IntCal20, 2 σ ** (cal AD/ BC)	Median probability (cal AD/BC) ^^	Laboratory no	Dated material	Published information	Reference	Point number on Fig. 9
25.95	south coast	3.5	Neka	outcrop	32.25	560	2400 ± 50	199 BC- 85 AD	50 BC		shell in grey and greenish mud	uncalibrated	Lahijani et al., 2009	
25.5	Hassan Gholi	7.8 (4.4)	TM	core	28	250	1497 ± 15	821–992 AD	910 AD	NZA-34283	shell in brown silt	830–981 AD (MAR09)	Leroy et al., 2013a, b; Kakroodi et al., 2015	
					30.25	475	2012 ± 24	328–481 AD (77%). 491–537 AD (8%)	400 AD	UBA-20606	shell in brown silt	278–443 AD (MAR09)		
25	inland	13 (9.6)	I	trench	26	top of kiln	933 ± 26	1300–1371 AD (65%). 1377–1424 AD (35%)	1350 AD	OxA-17,021	shell in brown silt layer	1344–1460 AD (MAR09)	Rekavandi et al. 2007; Sauer et al., 2013	9
24.16	inland	7 (11)	Cho	core	27.5	334	956 ± 24	1295–1411 AD	1350 AD	OxA-17,882	shell in fine grey sand	1325–1446 AD (MAR09)	Kakroodi et al., 2012	10
23.4	inland	12 (8.5)	S2	trench	23.9	50	959 ± 28	1292–1410 AD	1350 AD	Poz-97,351	black organic remains (plurimilimetric) from a grey clay	–	Leroy et al., 2022	11
					23.9	50	965 ± 28	1290–1408 AD	1350 AD	Poz-98,161	shell in grey clay	–		
23.02	inland	9 (12)	Agh	core	25.12	N/A	2303 ± 30	0–205 AD	80 AD	OxA-17,879	shell in coarse red sands	49–129 AD (MAR09)	Kakroodi et al., 2012	
23.56*	Hassan Gholi	21.4 (17.5)	C6	core	28.1	459	2410 ± 35	179 BC-67 AD	70 BC	Poz-51,065	shell in grey silt	193 BC-14 AD (MAR09 deltaR 26 yr)	Naderi Beni et al., 2014	
22.4	inland	12 (8.5)	V3A	core	23.7	131.5	817 ± 28	1397–1503 AD	1440 AD	Poz-93,406	shell in grey silt with oxydised spots and rootlets	–	Leroy et al., 2022	12
					24.4	197.5	845 ± 30	1393–1474 AD	1430 AD	Poz-106,200	shell at base of grey silt unit	–		
					25	267	2343 ± 31	60 BC-130 AD	30 AD	Poz-93,407	shell in brown silty sand	–		
					25.4	297.5	2377 ± 30	154 BC-83 AD	20 BC	Poz-93,408	shell in grey silt	–		
					25.7	331.5	2357 ± 32	112 BC-125 AD	10 AD	Poz-93,409	shell in grey silt	–		
22.06	S-E coast	2.1 (15.5)	Bagho	outcrop	22.06	N/A	2380 ± 35	163 BC- 83 AD	20 BC	Poz-19,943	organic matter in grey silt (bulk)	541–389 BC (IntCal09)	Kakroodi et al., 2012	3

b: from other regions of the Caspian Sea. ^ elevation according to Fig. 5 of Kroonenberg et al., 2007, ^^ rounded up, * FRO: 351 ± 33, ** only showing relative probabilities higher than 9% (rounded up).

| Elevation of dated level (m bsl)	Location name	Location details	Type of source	Environment	^{14}C BP	Calib 8.2, 2σ ** (cal AD/BC)	Median probability (cal AD/BC) ^^	Laboratory no	Dated material	Published information	Reference	Point number on Fig. 9
						IntCal20*						
24	*Turali, DAG LG*	HV04	Outcrop		2350 ± 43	153 BC-131 AD	**20 AD**	UtC 11,476	shell	240–70 BC (MAR04 RE 290 yr)	Kroonenberg et al., 2007	
25.15	*Turali, DAG OT21*	HVDag9B	Outcrop	lagoon clay	2370 ± 40	158 BC-121 AD	**10 BC**	UtC11617	shell	290–110 BC (MAR04 RE 290 yr)	Kroonenberg et al., 2007 Van de Velde et al., 2020	

Table 4 (*continued*)

b: from other regions of the Caspian Sea. ˆ elevation according to Fig. 5 of Kroonenberg et al., 2007, ˆˆ rounded up, * FRO: 351 ± 33, ** only showing relative probabilities higher than 9% (rounded up).

| Elevation of dated level (m bsl)	Location name	Location details	Type of source	Environment	^{14}C BP	Calib 8.2, 2σ ** (cal AD/BC)	Median probability (cal AD/BC)ˆˆ	Laboratory no	Dated material	Published information	Reference	Point number on Fig. 9
25.35ˆ	*Turali, DAG OT21*	HVDag11	Outcrop	lagoon clay	2322 ± 37	52 BC-20 7CE	**50 AD**	UtC11619	shell	190–50 BC (MAR04 RE 290 yr)	Kroonenberg et al., 2007 Van de Velde et al., 2020	
26.5	*Turali, DAG OT2*	HV01	Outcrop		2373 ± 38	158 BC-87 AD	**10 BC**	UtC 11,475	shell	440–290 BC (MAR04 RE 290 yr)	Kroonenberg et al., 2007	
26.5	*Turali, DAG OT2*	HV02	Outcrop		2366 ± 30	113 BC- 89 AD	**0**	UtC 11,423	shell	260–100 BC (MAR04 RE 290 yr)	Kroonenberg et al., 2007	
28	*Turali, DAG OT25*	HVDag8	Outcrop		2504 ± 34	360–273 BC (30%). 235–50 BC (66%)	**190 BC**	UtC 11,616	shell	280–260 BC (MAR04 RE 290 yr)	Kroonenberg et al., 2007	1
~ 42 to 37	*Kura delta, well 3*	10.55 m	Offshore core	Transgression after hiatus TS2/Derbent regression	1844 ± 32	530–651 AD (89%) IntCal20	**580 AD**	not provided	shell	541–615 AD (calibrated with reservoir 290 yr) IntCal13	Hoogendoorn et al., 2005	5
24.125	*Mazgah, core MZG*	212.5 cm	Onland core	20 cm above calcareous gytja with some foraminifera	1970 ± 35	47 BC - 128 AD	**50 AD**	Poz-30,615	tree leaves	44 BC-120 AD, average AD29	Ramezani et al., 2016	
24.425	*Langarud, core LL13VA*	298.5 cm	Onland core	wetland silt with Caspian dinocysts	638 ± 25	1288–1327 AD (43%) 1344–1395 AD (57%)	**1360 AD**	UBA-22965	rootlet	1285–1326 AD (41.3%), 1343–1394 (58.7%), med. Prob. 1355	Haghani et al., 2016	
24.655	*Langarud, core LL13VA*	321.5 cm	Onland core	wetland silt with Caspian dinocysts	535 ± 30	1324–1354 AD (22%) 1393–1437 AD (78%)	**1410 AD**	UBA-23788	rootlet	1318–1352 AD (25.1%), 1390–1438 (74.9%), med. Prob. 1408	Haghani et al., 2016	
24.975	*Langarud, core LL13VA*	353.5 cm	Onland core	wetland silt with Caspian dinocysts	585 ± 49	1298–1425 AD	**1350 AD**	UBA-27533	woody rootlet	1293–1423 AD (95.4%), med. Prob. 1352	Haghani et al., 2016	
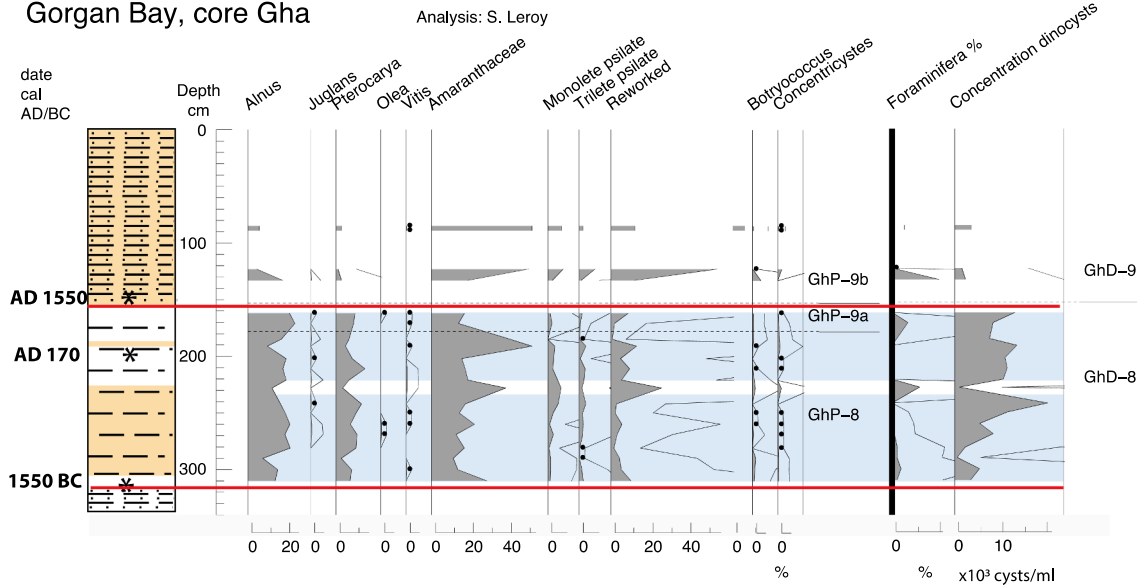
Fig. 3. Selected curves pollen and dinocysts for the top 336 cm of Gha core (full diagrams in SI). Dates shown (*) are the cal AD/BC median probability of the radiocarbon calibrated age range.

then the sediment at 184–176 cm is a brown sandy layer with sharp boundaries and shells at its base. The sediment is grey silt from 176 to 127 cm. Then an olive grey shell and silt layer is detected at 127–123 cm. Afterwards, an olive grey shell layer occurs at 126 cm and brown silt at 123–96 cm. The upper part of the core is an olive silt from 96 cm upwards. The MS varies from 10 to 80 10^{-5} SI with strong fluctuations. The MS variations of cores V4 and V5 do not seem to fit the oxidation

state of the sediment but are more likely related to changes in the detrital input. Three radiocarbon dates were obtained at the depth of 309.5, 184.5 and 126 cm, with a median probability of respectively cal 460 AD, 1210 and 930 (Table 4a). The calibrated age ranges of the last two dates do not overlap and are in a reversed sequence.

In core V5, ten samples barren in palynomorphs were documented below 200 cm depth (Figs. 2 and 5). Three further samples are barren in
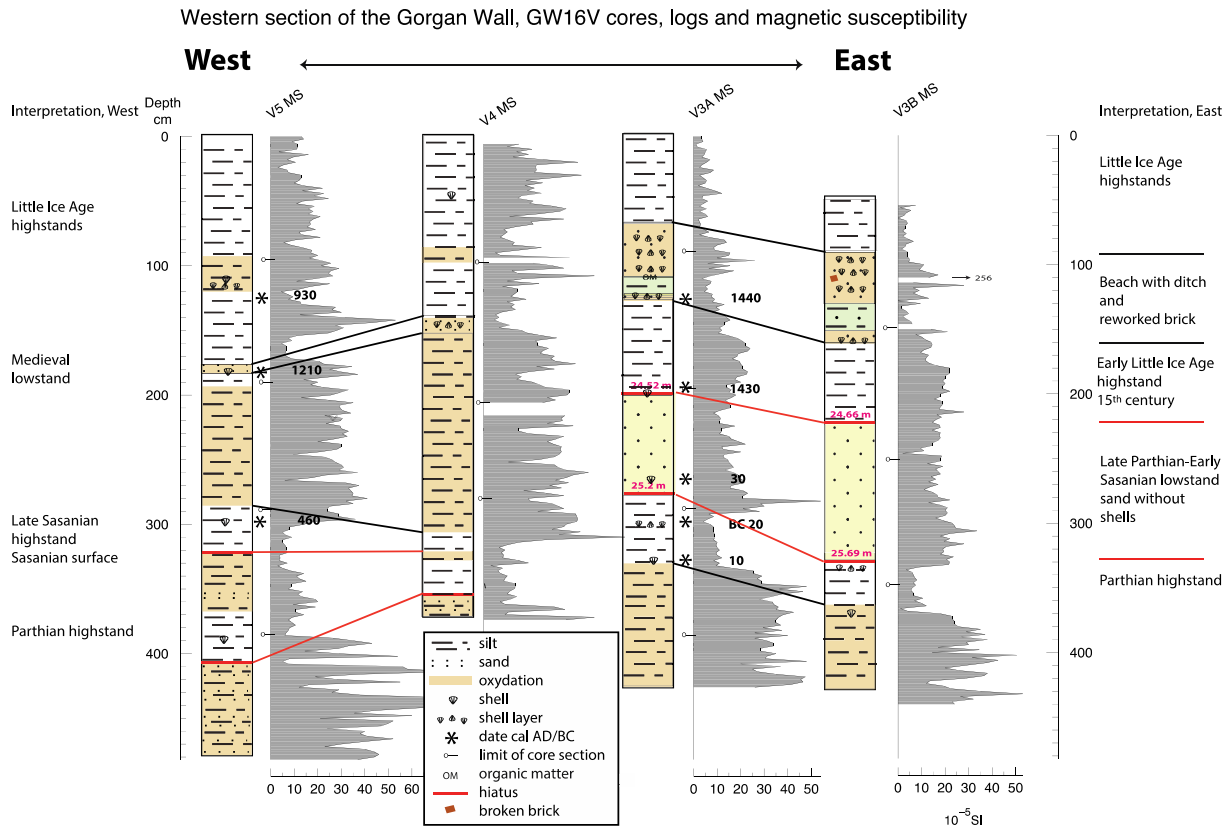
Fig. 4. Lithological logs of cores V5, V4 and V3. Magnetic susceptibility (MS) in 10^{-5} SI. Dates shown (*) are the cal AD/BC median probability of the radiocarbon calibrated age range.
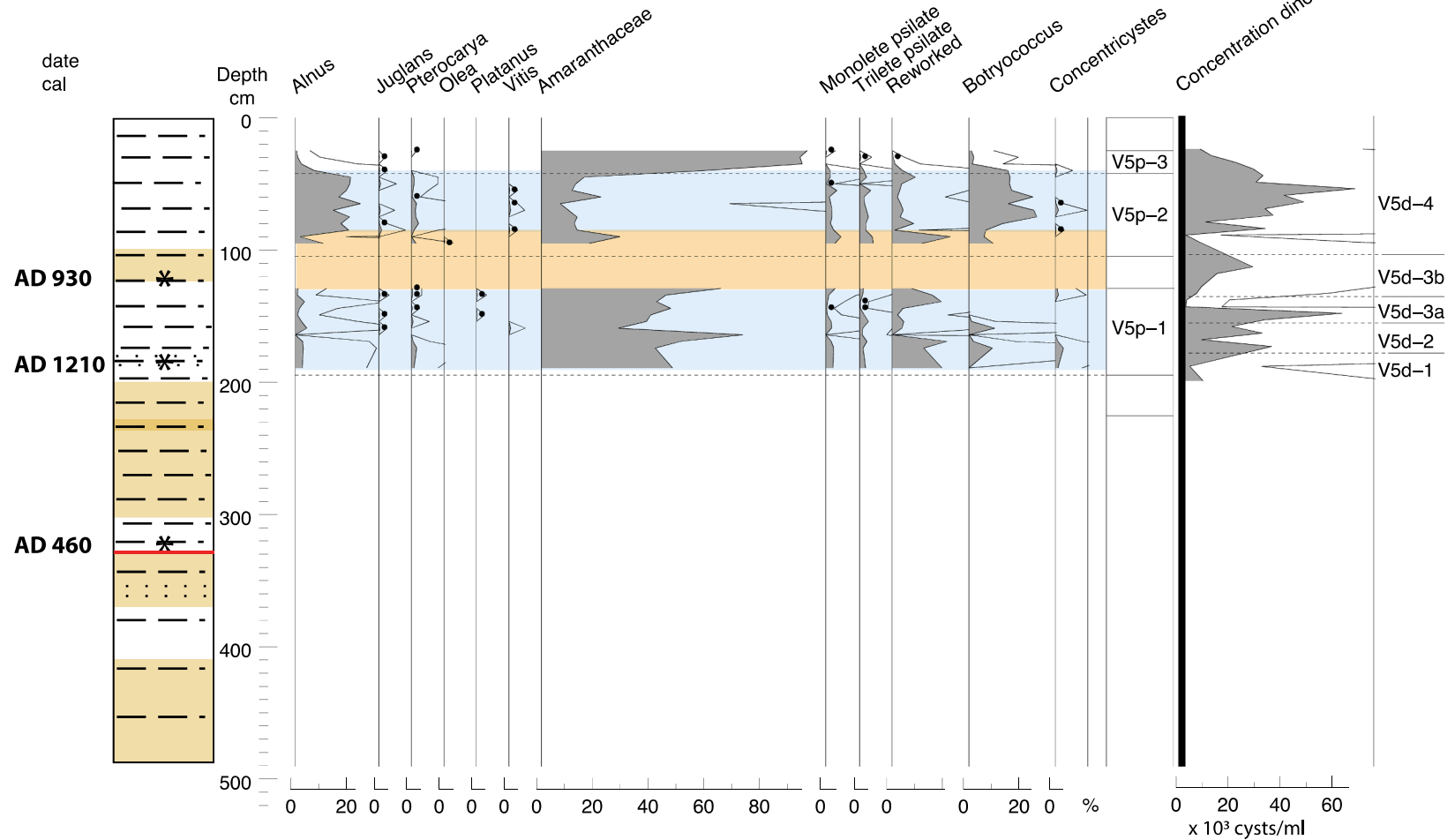
Fig. 5. Selected curves pollen and dinocysts of core V5 (full diagrams in SI) with magnetic susceptibility. Dates shown (*) are the cal AD/BC median probability of the radiocarbon calibrated age range.

pollen but unexpectedly produced good dinocysts assemblages (200, 119 and 114 cm). Concentrations are strongly fluctuating overall reflecting varying states of sediment oxidation.

In pollen zone V5p-1 (200–124 cm), Amaranthaceae dominate the spectra (Fig. 5 and SI 3). *Artemisia* are abundant too. In the arboreal pollen, *Quercus* has the highest percentages. *Pterocarya* are scarce. Reworked pollen percentages and concentration are fluctuating in opposite phase. Two samples between 124 and 104.5 cm are barren. In pollen zone V5p-2 (104.5–42.5 cm), the tree pollen is now very abundant with a strong development of *Carpinus betulus* and *Alnus*, alongside more moderate occurrences of *Quercus* and *Fagus*. *Pterocarya* percentages have picked up slightly. Amaranthaceae values have considerably dropped, while *Artemisia* retained the same values. Monolete and trilete spores are regularly present. Many indeterminable grains have been recorded. *Botryococcus* are abundant. In pollen zone V5p-3 (42.5–25 cm), Amaranthaceae values are extremely high, i.e. up to 95%. This has led to extremely high concentration values of nearly 138,000 pollen and spores/ml. *Polygonum aviculare-bistorta*-t. is present.

The dinocyst spectra are dominated by *I. caspienense* and L. *machaerophorum* B (Fig. 5 and SI 4). Small fluctuations between these two main taxa define four zones. Dinocyst zone V5d-1 (200–181.5 cm) has slightly more *I. caspienense* than L. *machaerophorum* B. A discrete but continuous occurrence of *S. cruciformis/G. etrusca* is noticed. Dinocyst zone V5d-2 (181.5–156.5 cm) has higher concentration values. The dominance of L. *machaerophorum* B characterises this zone. *S. cruciformis* A and L. *machaerophorum* ss are regularly present. Dinocyst zone V5d-3 a and b (156.5–136.5 cm and 136.5–104.5 cm) is characterised by sharply fluctuating dinocyst concentration values. More *I. caspienense* are seen at the start of this zone (zone 3a) and more L. *machaerophorum* B later (zone 3b). In dinocyst zone V5d-4 (104.5–25 cm), a dominance of

I. caspienense, with less instances of *S. cruciformis,* was recorded. *Caspidinium rugosum* is regularly observed as well as the bulbous form of L. *machaerophorum*. A slight increase of *S. cruciformis/G. etrusca* is detected. Concentration forms a bell-shape curve. The P/D ratio is very high at the end of this zone, i.e. at 25 cm depth.

In the lower meters of the V4 and V5 cores, two periods of emersion and hiatus (red lines in Fig. 4) are probable. They occur below a median age probability of cal 460 AD. This is followed by a period of sediment deposition that is unfortunately too oxidised to preserve palynomorphs. It is only above 200 cm depth that palynological diagrams are possible in core V5. Based on palynomorph preservation, it is proposed that two periods of presence of water are recorded. During the first period, the landscape is very open and the soils probably rich in salts. With caution, a possible age may be proposed although the two dates are inversed and do not overlap: perhaps centered over the first half of the eleventh century. Then a second high phase occurs, this time with the return of the natural coastal and highland forests in the plain and in the Alborz Mountains. It is attributed to the Little Ice Age highstand. The topmost samples indicate a deep degradation of the forest and the local redevelopment of desert conditions with a progressive shallowing and filling in of the site. The relatively fine-grained sediment facies suggests a lagoonal environment for both cores.

3.3. SE of the Hassan Gholi: top of core TM

We focus here on the top 660 cm of the long core TM, in order to assess environmental changes in approximately the last 2200 years. Lithology, radiocarbon dates and pollen were first published in Leroy et al. (2013a) and Kakroodi et al. (2015); but for the dinocyst counts, sums were increased over the whole 27.5 m of the sequence to allow building
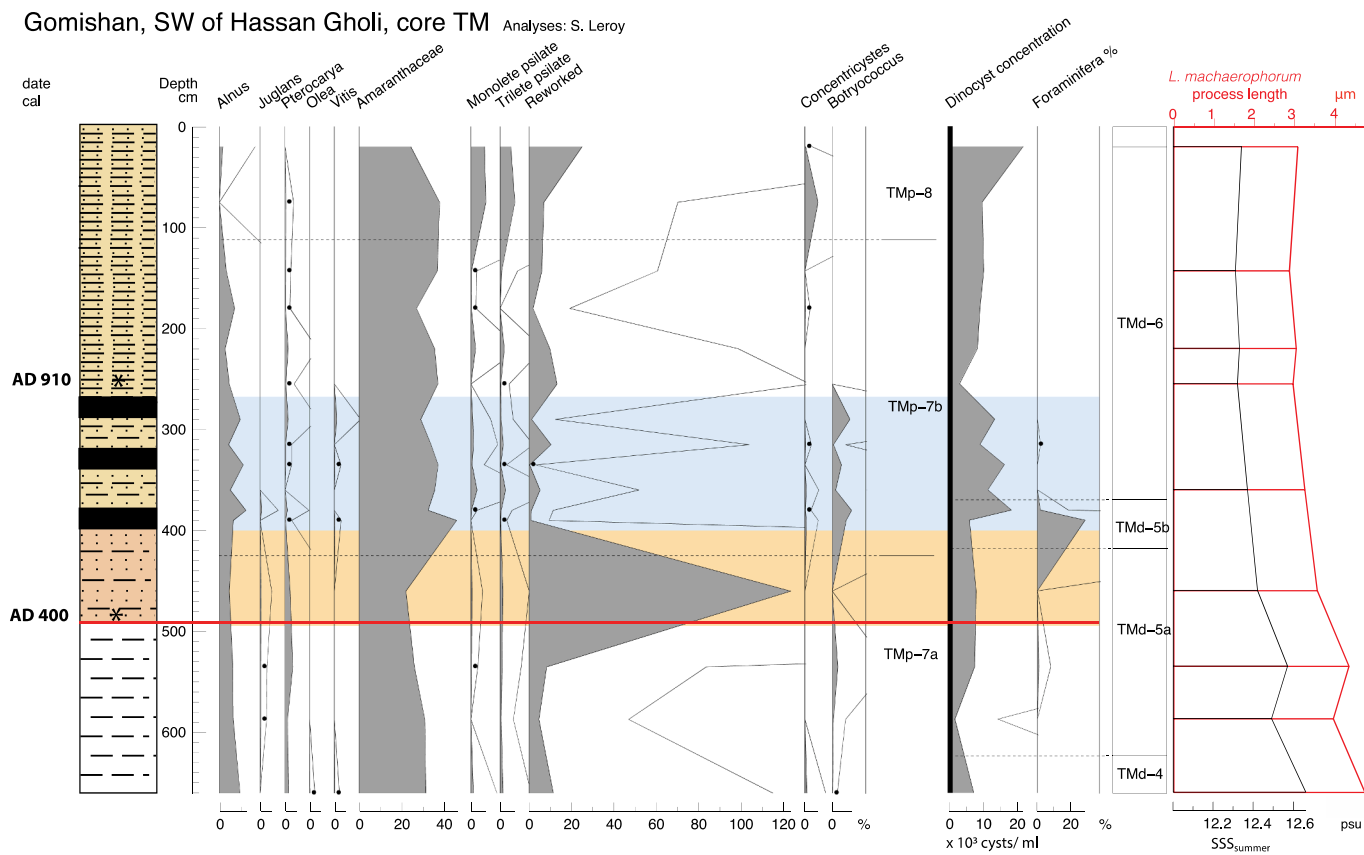

Fig. 6. Selected curves pollen and dinocysts for the top 660 cm of core TM (full diagram in SI) (analyses: S. Leroy). Reconstruction of sea surface salinity (SSS$_{summer}$) for the summer based on *Lingulodinium machaerophorum* processus length (measurements: K. Mertens). Dates shown (*) are the cal AD/BC median probability of the radiocarbon calibrated age range.

a separate dinocyst diagram (Fig. SI 7), as done for the other sequences of cores V5 and Gha.

In brief, the lithology is a dark to grey clay and silt becoming a mottled silt from 660 to 495 cm depth (Leroy et al., 2013a; Kakroodi et al., 2015). After a sharp change at 495 cm, the sediment becomes a very brown to reddish fine sand and sandy silt, with mottling. It is followed between 400 and 250 cm depth by three dark clayey silt units, with erosional features at the top of each of them with, in between them, fine silt to fine sand bearing signs of oxidation. Two radiocarbon dates are available, one at 475 cm with a median probability of cal 400 AD and one at 250 cm of cal 910 AD (Table 4a).

Pollen details (16 samples) have already been provided in Leroy et al. (2013a). In brief (Fig. 6 and SI 5): In zone TMp-7a and b, the landscape is very open with high amounts of plants from the desert and saline soils (most likely Chenopods in the family of the Amaranthaceae) and plants from the steppe. However, in zone 7b, a slight increase of *Quercus* is noticeable to the detriment of *Alnus* and *Carpinus betulus*. At the end of zone 7a, a very large peak of reworked elements is remarkable. It is derived from a sample taken in the reddish sands at 495–400 cm. In zone TMp-8, *Pinus* and *Quercus* increase. This may be due to a very recent plantation programme to re-afforest the region south of the Gorgan Plain. Also in the same zone, monolete and trilete spore percentages increase, illustrating the progressive infilling of the area by river sediment.

The dinocysts results for the top 660 cm are as follows (Fig. 6 and SI 6). In the last sample of zone TMd-4, at 660 cm (for the rest of this zone see fig. SI 6), the percentages of *I. caspiense* dominate the spectrum. *L. machaerophorum*, i.e. form B and ss, co-occur. High values of *Brigantedinium* sp. are observed. Relatively high values of *S. cruciformis*, 6–10%, are noted. In zone TMd-5, 623.5–370 cm, *I. caspiense* percentages stabilise around 40–50%. *L. machaerophorum* B continues rising but more slowly. After a progressive increase, *L. machaerophorum* ss, culminating in a peak at 19%, suddenly drops to 1% from subzone 5a to 5b. A fall of *Brigantedinium* sp. is noted across this zone. The P/D ratio fluctuates but is falling. In the last sample of this zone, a peak of foraminifera linings is observed, already present in low quantities from the base of zone 5a. Zone TMd-6, 370–20 cm, is characterised by a maximum of L. *machaerophorum* B (49%). While L. *machaerophorum* form B remains high, form ss remains low. *Brigantedinium* sp. are quasi absent. *S. cruciformis* is still present. The P/D ratio is low to very low. The reconstruction of the sea surface salinity for summer suggests during the interval between 660 and 535 cm, a SSS$_{summer}$ of 12.5–12.7 psu, thus higher than later in the sequence, and a progressive return to current conditions of 12.3 psu at the depth of 20 cm (Fig. 6 and SI 7).

The interpretation of the top 660 cm of the TM sequence indicates an increased salinity in comparison to below this depth, with the maximum of SSS$_{summer}$ at 660 and 535 cm and the progressive increase of L. *machaerophorum* ss up to a maximum of salinity at 460 cm (sample in the sand at 495–400 cm). The sand itself is a clear sign of emersion, a probable beach. This horizon contains many reworked elements. A shell taken close to its base indicates an age of cal 328–537 AD. Just above the sand comes the three dark clayey silt horizons attributed to lagoons.
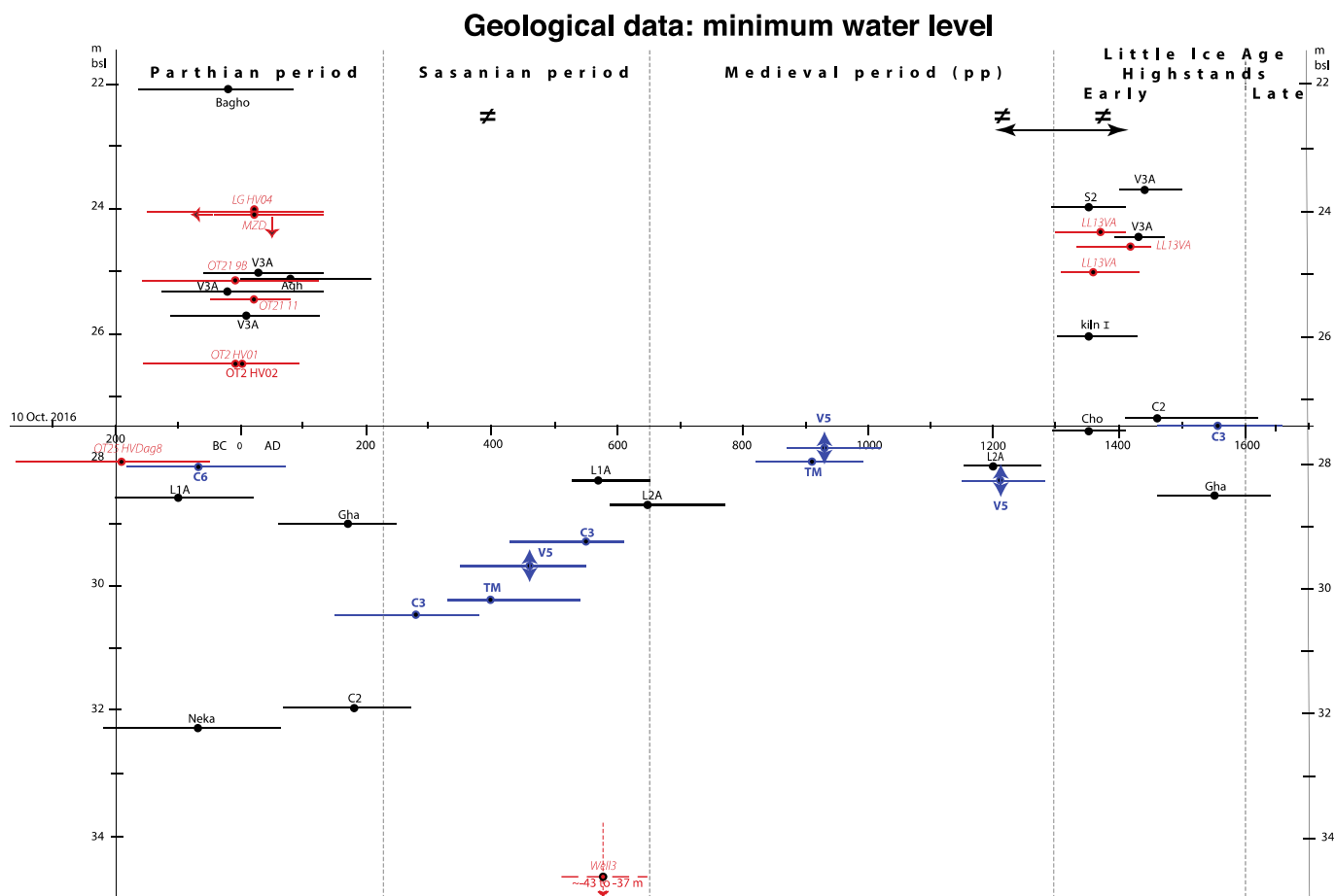

Fig. 7. Water elevation compilation of geological sequences. The x axis showing time is positioned at the water level of 10 Oct. 2016. In blue and bold: sites from Hassan Gholi. In red and italics: sites outside the SE corner of the Caspian Sea. Crossed equal signs: Amu Darya diversions according to Létolle and Mainguet (1993), Létolle (2000) and Sala (2019). Black horizontal line with two arrows for period of likely diversions according to Boroffka (2010). Double vertical arrows for uncertainty in elevation. Simple arrows pointing down and left for MZG for minimum age and elevation. pp.: pro parte. (For interpretation of the references to colour in this figure legend, the reader is referred to the web version of this article.)

Only one sample was taken in it, which displays high values of foraminifera. The last meters reflect the lagoon infilling locally. The increase in river indicators in the pollen and spore assemblages fit well with a slight decrease of SSS_{summer}.

3.4. Transects and radiocarbon dates from other places

A west to east transect, reaching the westernmost known section of the Gorgan Wall consists of four cores, i.e. V5, V4 and V3A and B (Fig. 4). Visually, it is clear that the sand levels at 184–176 cm in core V5 and at 148–142 cm in core V4 correlate. The grey silt above a sharp lithological in core V5 at 323.5–298.5 cm correlate well to 321.5–308.5 cm in core V4. The correlation of the parallel cores V3A and V3B is clear owing to a thick sand layer devoid of shells around 300–200 cm depth dating to the Late Parthian-Early Sasanian lowstand and owing to a gully filled in with a lacustrine greenish silty clay around 120 cm depth dating from the 15th century (Leroy et al., 2022). It seems that the sediment deposition (lagoon facies) observed in core V5 between cal 348–550 AD and around the 9th to 13th century did not reach far inland, as absent in cores V3. In cores V3A and B, furthest inland, only high highstands are indeed recorded, i.e. before the Sasanian lowstand, most likely a highstand in the Parthian period (the age of the whole Parthian period is 247 BC to 224 AD) and a second highstand in the Little Ice Age (LIA).

A transect from the edges of the Gorgan Bay to the SW corner of the Hassan Gholi, passes through core V5 (Fig. 2). Based on lithological signs of hiatus and/or emersion, the Sasanian surface (the surface on which the walls were built; see Leroy et al., 2022) is located at 155 cm depth in core Gha, at 323.5 cm in core V5 and between 495 and 400 cm in core TM. The TM sand (corresponding to the Sasanian surface) is poorly dated at 328–537 AD and the return of water is dated immediately afterwards at cal 348–550 AD in core V5.

Below the Sasanian surface, the sediment shows a period of highstand with many fluctuations in cores Gha and V5, but more stable in core TM in the Hassan Gholi. After the Sasanian surface, several periods of highstands are noted.

The sites in the Hassan Gholi area (cores V5, V4, TM and cores C3 and C6 from Naderi Beni et al. (2013, 2014); Fig. 1c) indicate higher elevations than expected. This can be explained by the lagoon being at times separate from the Caspian Sea and influenced by the Atrek River and other freshwater inflow. These sites should therefore be discussed separately from CSL and are thus shown in blue and bold in Fig. 7 and Tables 4a and b. The sediment of core TM is oxidised from 495 cm upwards suggesting shallow waters. A hiatus at 323.5 cm in core V5, already correlated in the transect with the sand of core TM. The group of dates (Fig. 7) shows that during the Sasanian lowstand and the Medieval period, the lagoon remained filled with water.

A lagoon and barrier complex has been studied in detail in Turali (Dagestan) with radiocarbon dates and precise elevations (Fig. 1b). Five dates (recalibrated) fall between 158 cal BC and cal 207 AD, for elevations above the present, i.e. -24 to − 26.5 m (Kroonenberg et al., 2007) (Table 4b). One additional earlier date at 360–50 cal BC indicates slightly lower elevation at − 28 m (Kroonenberg et al., 2007) (Table 4b).

In Well 3 of the Kura Delta, a transgressive surface TS2 follows a shell-rich horizon (dated at 580 AD, median probability) interrupting massive clays and silts (Table 4b) (Fig. 1b). With the support of inferences from other cores in the same study, it was suggested that this lowstand reached − 42 to − 37 m (Hoogendoorn et al., 2005). This lowstand was attributed to the Derbent lowstand (Derbent in Russian, Darband in Persian) (Rychagov, 1997).

The Mazgah mire, along the coast, is a coastal wetland mostly isolated from the sea (Ramezani et al., 2016) (Fig. 1b). Tree leaves dated at 20 cm above a thin lagoonal horizon provided an age of 47 cal BC–cal 128 AD (Table 4b). The arguments for a lagoonal highstand are some indicators of changes from an alder carr to a slightly brackish environment (e.g. with foraminifera) and slightly deeper water. This is followed by a progressive regression.

Cores taken in the Langarud wetland, > 11 km from the current coastline, contain a terrestrial record interrupted by a brackish level (dinoflagellate cysts in an otherwise terrestrial context; Haghani et al., 2016) (Fig. 1b). Three ^{14}C dates suggest that the CSL rose to −25 and to −24.4 m in the 14th century and at the beginning of the 15th century respectively (Table 4b).

3.5. Geological data and Caspian Sea levels

Thirty radiocarbon dates (with error bars lower than ±50 yr) were collected in a rather restricted geographical area of 125 km W-E by 50 km N-S in the SE corner of the Caspian Sea (Table 4a; Fig. 7), to which another eleven dates from other areas may be added (Table 4b).

At the start of the Parthian period, a site indicates elevations around −28 m (Turali) (Fig. 1b). In the middle of the Parthian period, quite clearly many sites suggest a highstand, with Bagho showing the highest elevations and largest penetration inland: −22.06 m (Fig. 7, Table 4a and b). Then the water level falls relatively quickly, reaching perhaps already levels below the present before the end of the Parthian Period. In the Early Sasanian period, this fall probably carries on, we have no sites, except one in the Hassan Gholi at quite a low elevation. Clearly though in the mid-Sasanian period, the levels are very low. Hoogendoorn et al. (2005) have suggested that the level reached −37 to −42 m. But two caveats need to be taken in consideration: 1) the hiati in Well 3 and Piston Core 5 of the Kura Delta can be interpreted as an emersion feature below a transgressive surface (TS2) (coastal to onshore setting; Hoogendoorn et al., 2005), if a mass movement linked to a sea level drop can be excluded; and 2) a reasonable estimations of the water column is difficult to make at the scale necessary to fine-tune to historical evidences, as it is hard to distinguish between 5 and 10 and 15–15.5 m. At the end of the Late Sasanian period or shortly after, the levels re-increase abruptly and reach −29 to −28.5 m. In the Medieval period, hardly any geological information is available, perhaps due to low levels and absence of sedimentation along the coasts. One sample, at the end of this period in core L2A, shows a level at a minimum of −28.1 m in cal 1149–1274 AD. In the early LIA, the levels have clearly re-increased as shown by several sites, reaching at least −23.7 m. The increase might have been sharp at cal 1350 AD (median probability) as three sites spread from −27.5 to −23.9 m. Then the levels may have fallen again to −27.3 m or even −28.5 m.

4. Part 2: archaeo-historical data

4.1. Introduction

Over 35 historical datapoints (Table 5 and Fig. 8) were used; they were taken from the 2013 curve (Naderi Beni et al., 2013), verified one by one and completed by additional reading.

The last 2200 years are divided in four periods. Two periods are named here according to Persian history, i.e. Parthian (247 BC to 224 AD) and Sasanian (224 AD to 651) periods because, for a large part of the time concerned, the south Caspian basin, including up to part of Dagestan (Middle basin of the Caspian Sea), was under the dominion of Persia. Then the "Medieval" term is used, corresponding to the Arab Conquest, in preference to the Derbent period (see discussion). Strictly speaking from a historical point of view, the Medieval period extends from 651 AD to 1500. However, for practical reasons, in the Medieval section, we only discuss the points until 1300 AD, i.e. the starting date of the LIA in its extensive definition. Finally, the name of a climatic phase is used for the last centuries, i.e. the early and late Little Ice Age. At a global scale, a wide definition of the LIA gives its start at 1300 AD (Mann, 2002; Mann et al., 2009). Moreover, we divide the LIA in early LIA, i.e. at 1300–1600 AD and in late LIA at AD1600–1850.

Table 5
Archaeological and historical data with their elevation and dating information.

Historical period	Location	Feature		Elevation in m bsl	Age	Symbol in figure	Reference	Letter point on Fig. 9
Parthian	N. coastline	maps of Erastosthenes and M. of Tire	water level lower than present	32	2nd century BC	box	Varushchenko et al., 1987	a
Parthian	_	archaeology	no precision	32	1st century BC	box	Apollov in Karpychev, 2001	
Parthian	_	burials	above water	31.7	1st century BC	box	Appolov in Varushchenko et al., 1987	
Parthian	_	archaeology	no precision	~27	~1 AD	dot	Karpychev, 2001	
Parthian	from Apsheron to Makhachkala	coastline	not available to travellers	22.5	1st century AD	box	Varushchenko et al., 1987	b
Sasanian	Khwarazm	irrigation system	destruction	_	380–400	≠	Létolle and Mainguet, 1993	
Sasanian	Gorgan Bay	Tammisheh Wall	buried wall	31.5	5th century AD	box	Bates et al., 2022a	c
Sasanian	Derbent	wall	construction	33.8	6th century AD	box	Kudrjavcev and Gadžiev, 2002	d
Sasanian	S-E coast	Gorgan Wall	buried wall	N/A	6th century AD	_	Sauer et al., 2022	
Sasanian	Derbent	fortress	buried amphora	32	6th century AD	box	Varushchenko et al., 1987	
Sasanian	Volga	channel in delta	cultural layer	31.7	6th century AD	box	Varushchenko et al., 1987	
Medieval	Derbent	wall	partial restauration	31	705–715	dot	Varushchenko et al., 1987	e
Medieval	Derbent	harbour	extension of breakwater	29	747–750	dot	Varushchenko et al., 1987	f
Medieval	Derbent	wall	history & geomorphology	28 to 30	8-10th century AD	box	Varushchenko et al., 1987	
Medieval	Derbent	wall	distance to the sea	35 to 36	943–945	box	Varushchenko et al., 1987	g
Medieval	Baku	caravanserai	submersion	<30.4	1100–1150	box	Brückner, 1890	h
Medieval	Urgench	dam	destruction	_	1219–1221	≠	Létolle, 2000	
Medieval	Derbent	caravanserai	building	31	1234	dot	Karpychev, 2001	i
Early LIA	Abeskun Town	port	submersion	22	1303	dot	Varushchenko et al., 1987	
Early LIA	near Kura delta	Bayandovan settlement	flooding	28	1305–1306	dot	Karpychev, 2001	j
Early LIA	Lankaran	S. Zahed tomb	in danger of flooding	<16	1306–1320	dot	Brückner, 1890	k
Early LIA	Lankaran	S. Zahed tomb	on shoreline	22	1306–1307	dot	Varushchenko et al., 1987	l
Early LIA	Urgench	dam	destruction	_	1372–1388	≠	Sala, 2019	
Early LIA	Baku	fortifications & mosque	submersion/close to sea	26 to 25	14th century AD	box	Varushchenko et al., 1987	m
Early LIA	Derbent	wall	emersion	27 to 28	1474–1478	box	Varushchenko et al., 1987	n
Early LIA	_	two maps	_	26.5 to 29	1556 & 1558	box	Varushchenko et al., 1987	o
Early LIA	Terek Town	at mouth of Stari Terek channel	Terek town foundation	26 to 29	1588	box	Varushchenko et al., 1987	p
Early LIA	Derbent	wall	emersion	29	1590	dot	Varushchenko et al., 1987	q
Early-Late LIA	Derbent	additional tower building	water line retreat	28.5	1587–1606	box	Karpychev, 2001	r
Late LIA	Terek Town	_	distance to river mouth	25.3	1604	dot	Varushchenko et al., 1987	
Late LIA	Chechen Island	_	distance to coastline	25.3	1604		Varushchenko et al., 1987	
Late LIA	Derbent	fort	construction	23 to 24	1606–1629	box	Varushchenko et al., 1987	s
Late LIA	Terek Town	town	distance to coastline	25 to 24.5	1623	box	Varushchenko et al., 1987	t
Late LIA	Gorgan Bay	Ashraf harbour	construction	23.5	1628	dot	Naderi Beni et al., 2013	u
Late LIA	Derbent	wall	markings	21.3	1638	dot	Brückner, 1890	v
Late LIA	Derbent	wall	not in the sea	23	1638	dot	Varushchenko et al., 1987	w
Late LIA	Derbent	wall	not in the sea	24	1668	dot	Varushchenko et al., 1987	x
Late LIA	Terek Town	town	displacement due to flooding	24	1668		Varushchenko et al., 1987	x
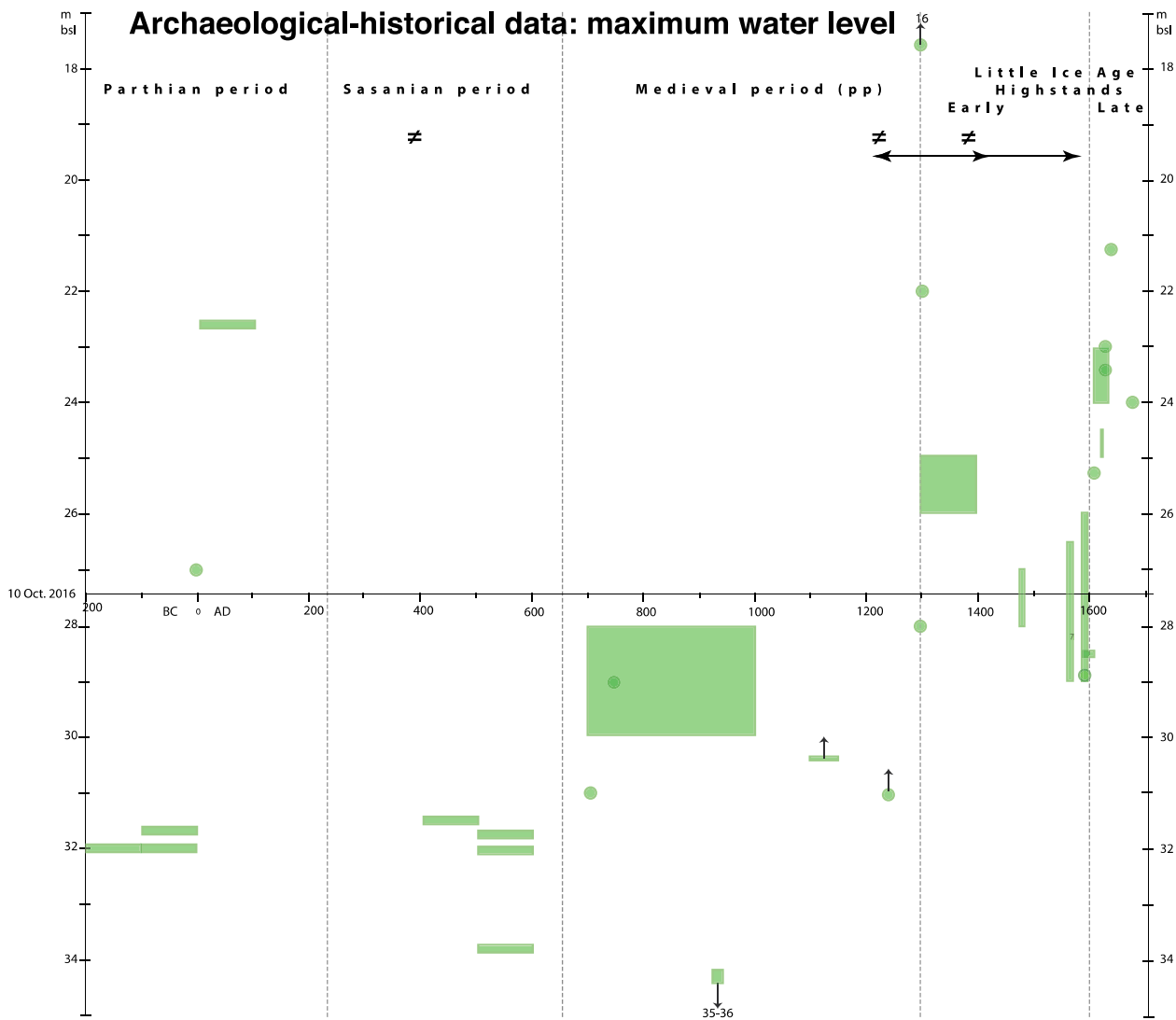
Fig. 8. Water elevation compilation of archaeological and historical data over time. The x axis showing time is positioned at the water level of 10 Oct. 2016. Crossed equal signs: Amu Darya diversions according to Létolle and Mainguet (1993), Létolle (2000) and Sala (2019). Horizontal lines with two arrows for period of likely diversions over 1221–1417 AD according to Boroffka (2010) and over 1221–1575 AD according to Herzfeld (1947). Arrows pointing upwards for minimum elevation. Arrows pointing downwards for elevations out of the axis range used here.

4.2. Relevance of the Amu Darya lower reaches

For the reconstruction of CSL, it is important to look at what happened in the Amu Darya and Syr Darya deltas. The Amu Darya has been called a Caspian river by some, as, over its existence, it has flowed mostly to the Caspian Sea. Artificial irrigation has been practiced in the Khwarazm (Chorasmia) between Amu Darya and Syr Darya for a very long time. It developed quite extensively with some very large earthen dam building at least since the 6th century BC when Khwarazm became part of the Persian empire (Létolle, 2000; Boroffka, 2010). The main river flow of the Amu Darya (left branch in Urgench, the right one still going to the Aral Sea) was diverted to the Sarykamish Lake (at a much lower elevation than the Aral Sea; Herzfeld, 1947) and from there to the Caspian Sea via the Uzboy River (Fig. 1a). Herzfeld (1947) indicates that the idea of artificial river diversion is extremely old. In the 3rd century BC, Patrocles, a Greek military man and engineer, was sent to the Urgench region to explore the possibility of a commercial route between the Black Sea and India. This also indicates that the Amu Darya was connected to Caspian Sea at that time (Herzfeld, 1947). There are at least two mentions of the Uzboy being possibly navigable by ships: in the 4th century BC by Aristobolus, a historian and companion on Alexander

the Great campaigns, although some confusion with the Sarykamish or other seas/lakes cannot be excluded (Thorley, 1969) and in 1392 AD and following decades by several authors (Létolle, 2000; Boroffka, 2010). Historical documents also pinpoint that between the 10th and the 13th centuries, the Uzboy had no water because of a major dam built on the main feeding arm to the Sarykamish (Gloukhovskoy, 1893).

The hypothesis that river diversion could strictly be caused by human mediation (for benefit or by war) has however been challenged by Toonen et al. (2020), and a climatic contribution has been highlighted (see climatic discussion below). In any case, in addition to diversions, dams create vulnerabilities not only to potential enemy attacks but also to natural hazards (such as earthquakes), which may cause sudden dam breaches.

4.3. Parthian Period

From Varushchenko et al. (1987) and Karpychev (2001), we learn that the CSL in the second and first centuries BC was below the mark of −32 m; this is based on archaeological data. However, 2000 years ago, it is likely that the sea level was not higher than it is now (Karpychev, 2001). In the first century AD, the coast between Apsheron and

Makhachkala (Dagestan) was flooded becoming unavailable to travellers, thus a CSL of − 22.5 m was suggested (Fig. 1b) (Varushchenko et al., 1987).

4.4. Sasanian Period

According to Dimishqui, the town of Abeskun, a famous ancient trade centre at the SE corner of the Caspian Sea, was founded by king Kavad I (488–531 AD; this is a revised and more correct date than that cited by Varushchenko et al. (1987)), and is likely to be the successor of the more ancient town of Socanda, attested by Ptolemy and Ammianus Marcellinus in the 2nd and 4th centuries AD (Sauer et al., 2013). It has been proposed that it corresponds to modern-day Gomish Tappeh near Gomishan but location of the town and/or its harbour may have shifted repeatedly and may have been in the 5th–6th centuries in an area now offshore of Gomishan, when the CSL were low (Varushchenko et al., 1987; Zonn et al., 2010; Naderi Beni et al., 2013; Sauer et al., 2013) (Fig. 1b). So, although relatively well documented, the absence of elevations hinders its use for CSL reconstruction.

The renowned Sasanian walls, i.e. the Gorgan (>170 km long) and Tammisheh (>12 km long) Walls in Iran, were built to protect the southern farmers from the northerners (especially the Hephthalites or White Huns). One of the long walls, the wall of Tammisheh, ends in the Gorgan Bay (Fig. 1). It carries on below the current water level and was built, as the other ones, around the 5-6th century AD when the water level was lower than present around − 32 to − 31.5 m (Nokandeh et al., 2006) (Table 4b). The Tammisheh Wall, if the terminus was indeed found, ended on the then shoreline or abutting the thalweg of the Qareh Su (a west-east river at the same latitude) (Leroy et al., 2022). Given the shallow gradient and the lack of stone, it would have been impossible to continue it to 2 m water depth (Sauer et al., 2013). The Derbent Wall (Dagestan) was built around the 6th century and also has a terminus below current water level (Kudrjavcev and Gadžiev, 2002). Interestingly the Derbent Wall (built on a slope) terminates around 2 m below the 6th-century water level to make bypassing it impossible. A buried layer with cultural artefacts found in the Volga Delta at − 31.7 m completes the picture (Varushchenko et al., 1987).

Létolle and Mainguet (1993) evoke the possibility of hydraulic infrastructure (including dams) destruction in northern Turkmenistan by Huns (not Hephthalite) in 380–400 AD. However, the impact on the Amu Darya on the CSL must has remained minor. The date certainly does not fit the chronology of the Derbent and Tammisheh Wall flooding (see below), nor does it fit the geological data collected around the Caspian Sea.

4.5. Medieval Period (pro parte)

Abundant information is derived from observations on the Derbent Wall and Derbent caravanserai as well as a caravanserai in Baku, such as distance to the sea, destruction by the sea or construction of additional buildings (Table 5).

The then resplendent town of Gurganj (Kunya Urgench in Khwarazm) and related irrigation infrastructure were often destroyed during wars (Fig. 1a). For example, Genghis Khan's army (led by his sons) fought in 1219–1221 AD and in an act of revenge caused a lot of destruction, including that of a major dam built in the 10th century on the Amu Darya (Létolle, 2000; Naderi Beni et al., 2013). The river waters ran into the Uzboy, reached the Caspian Sea and caused a well-documented temporary increase of the water level by ~7 to 9 m (Herzfeld, 1947; Naderi Beni et al., 2013; Krivonogov et al., 2014).

4.6. The early and late Little Ice Age

Abeskun was an important coastal town until 1303–1304 AD (early LIA) when its harbour was swallowed by the Caspian Sea. It became an island and finally disappeared below the water (Varushchenko et al.,

1987; Naderi Beni et al., 2013). Also in these more recent times, no elevation points are available. More relevant information is derived from the tomb of Sheik Zahed in Lankaran, fortifications in Baku, flooding of a settlement near the Kura delta, changes to the Derbent Wall and observations on the position of the town of Terek in the Terek Delta (see Table 5; Fig. 1b).

A renewed and final destruction of Urgench and of a major dam by the Timurid Mongols (1372–1388 AD) may have contributed to high levels in the Caspian Sea (Létolle and Mainguet, 1993).

In the late LIA, information is provided by observations in Derbend and Terek, in addition to the appearance/disappearance of islands. The remains of an old port, i.e. the Ashraf Port, of the Safavid era (1501–1722 AD) constructed in 1628 AD were found at an altitude of −23.5 m in the plain of Behshahr (Naderi Beni et al., 2013), reflecting higher than present CSL. The harbour was connected to the then known world through the Royal Road and the Silk Road (Nadim and Zahedi, 2018).

5. Part 3: Discussion

5.1. An updated water level curve

Here we juxtapose the results from our two previous compilations, i. e. geological data set and archaeo-historical data set, in order to derive a new robust and more complete CSL for the last 2200 years. Their joint distribution over time reveals a series of similar low and highstands (Fig. 9a, SI 8 and table SI 1). The small numbers on Fig. 9a allow linking to points chosen in Tables 4 and 5. Often, but far from always, the geological data are lower than the archaeo-historical data as, as underlined earlier, the geological data indicate a minimal elevation, and the archaeological ones provide an upper limit. It has been necessary to treat separately the data from the Hassan Gholi as their elevation values were generally higher. This can be explained by the usually higher elevation of the water body with regard to the Caspian Sea, owing to a different water balance. One has to recognise however that 1) sediment compaction has played a role, affecting increasingly more sediment as it gets older; and 2) seismic movements have affected both sets of data, upwards and downwards (for the latter see discussion in Section 5.3.1). Highstands and lowstands are identified in relation to present-day water levels shown in Figs. 7 and 8 as the x axis.

5.1.1. The mid-Parthian highstand

During this period, a brief highstand but very well illustrated at ca >50 BC to ca AD >50 by geological data in multiple sites around the Caspian Sea and by historical signs of flooding around the western coast. The highest points are at the Bagho outcrop at −22.06 m, and along the western coast at ~-22.5 m.

This is preceded by a poorly documented lowstand and followed by another lowstand. Old maps in the 2nd and 1st century BC, burials in the 1st century BC indicate low levels, perhaps as low as −32 m. A radiocarbon-dated point in core L1A belongs probably to this lowstand. Towards the end of the Parthian period, the level falls anew. It is only shown by dates in cores Gha and C2, suggesting −32 m at 180 AD.

5.1.2. The mid-Sasanian lowstand

The Sasanian period starts with a lack of data over ~270 years (between 180 AD to 450). By integrating levels before and after this long period, one may suggest, with caution, falling levels. Some evidence suggests then very low levels: 1) Tammisheh Wall in the 5th century AD, its likely terminus being at ca −31.5 m (Bates et al., 2022a) and 2) the initial construction of the Derbent Wall in the 6th century, terminating at −33.8 m, its mortar-less construction beneath −32 m suggesting that it continued into the sea beyond the then water level of −31.5 to −32 m (Kudrjavcev and Gadžiev, 2002). These very low levels may be related to the TS2 hiatus found in the Kura delta core at −42 to −37 m (depths pending caveats above-mentioned) dated by a radiocarbon date with a
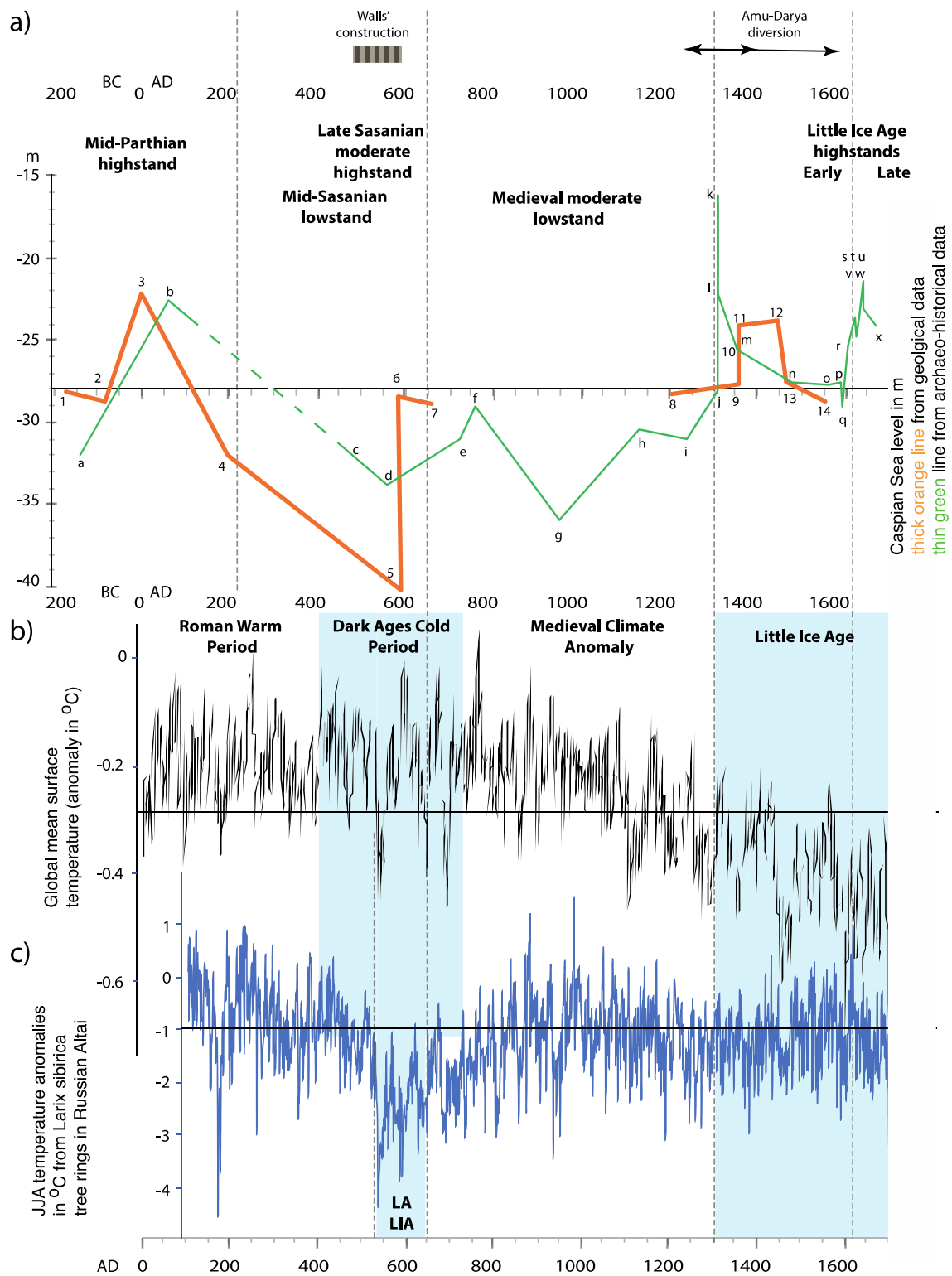
Fig. 9. Caspian Sea levels and climate. LALIA: Late Antique Little Ice Age.

a: Overlap of the two sets of data to produce final sea level curve in meters below sea level in reference to the Baltic 1977 datum. Horizontal line at sea level of 10 October 2016, i.e. -27.45 m. Horizontal lines with two arrows for period of likely diversions over 1221–1417 AD according to Boroffka (2010) and over 1221–1575 AD according to Herzfeld (1947). Rectangle with vertical lines indicates the Sasanian Walls' construction period. Small numbers and letters on the curves refer to points highlighted in Tables 4a, b and 5, and synthesised in table SI 1.

b: Global Common Era mean surface temperature (anomaly in °C compared to present-day). (PAGES 2k Consortium et al., 2019). Arbitrary horizontal line. Light blue boxes for cold periods.

c: June–July–August (JJA) temperature anomalies in °C compared to present-day from *Larix sibirica* tree rings in Russian Altai (Büntgen et al., 2016). Arbitrary horizontal line. Light blue boxes for cold periods. (For interpretation of the references to colour in this figure legend, the reader is referred to the web version of this article.)

wide age range at cal 436–651 AD. These data indicate a dramatic water level fall in comparison to the Parthian highstand, by at least 11 m (archaeological data), or perhaps even more (geological data); this is the mid-Sasanian lowstand. The Sasanian surface has been crossed by several sediment cores in the Gorgan Bay. Their study confirmed the CSL at the time of the Tammisheh Wall terminus construction at − 31.5 to − 32 m (Leroy et al., 2022). The lowstand may have led to a situation when large land expanses (due to the shallow underwater slope) were suddenly emerged and vulnerable to northern invasions.

Hassan Gholi, a water body to the north of the Gorgan Wall, was several meters higher than the Caspian Sea. The movement of its shoreline would have affected the western terminus of the Gorgan Wall. It explains why three diverging walls appear in the western section of the wall (Bates et al., 2022b).

If we accept the depth of − 32 m in the late 5th and in the 6th centuries, it seems that the walls and their termini were built when the sea level was already re-increasing and certainly not decreasing (see next section), otherwise the wall termini would have been found at an even lower elevation.

5.1.3. The Late Sasanian or early post-Sasanian moderate highstand

The Late Sasanian or early post-Sasanian highstand was of moderate amplitude, i.e. ~-28.5 to − 29 m, thus slightly below current water level. But it was high enough to flood the lower parts of the walls. Evidence comes from two levels in cores L1A and L2A from the Gorgan Bay. It seems to have occurred at some stage between the 6th and the 8th century AD, i.e. towards the end of the Sasanian era or in the early post-Sasanian era.

5.1.4. The medieval moderate lowstand

This long lowstand (>600 years) is not well illustrated in the geological data: i.e. two points, one at the very start at − 29 m and towards the end at − 29 m again. Three data points from Hassan Gholi are just below current sea levels.

The lowstand is proposed here mostly on the base of historical data. It is hard to decide if the lowstand is limited to the depth of − 31 to − 28 m, or the very low values of − 35 to − 36 m at 943–945 AD should be accepted. The latter is based on the distance to the sea of the Derbent Wall. The tenth century is also the period of the main dam building on the Amu Darya, thus not allowing a water flow towards the Sarykamish anymore. In general, a paucity of evidence for a very low level in the Medieval times thus invites caution.

5.1.5. The LIA highstands

The early LIA highstand is illustrated by more than seven dates here and many historical observations. It starts by an extremely high-water level, perhaps as high as 16 m, if the flooding of Sheik Zahed tomb is to be considered at 1306–1320 AD. Other historical information seems to support a peak at least until − 22 m at 1303–1307 AD in the Kura delta and Lankaran. Then the level remained higher than present close to − 26 to − 25 m in the 14th century as seen from a range of evidence in Baku (tower wall flooded and sea approaching the mosque). Several geological data indicate a clear peak a little later (between cal 1350 AD and 1440, median probabilities) at − 23.7 to − 23.9 m, this includes the flooding the western terminus of the Gorgan Wall (as seen by the flooding of a kiln), but certainly linked to the more precisely historically-dated peak of 1303–1307 AD. This followed by a progressive fall to − 29 m in 1590 AD.

In the late LIA, radiocarbon dates are not used, as the limit of their meaningful application is reached. According to historical observations, the level re-increases abruptly to reach − 21.3 m at 1638 AD. In 1668 AD, several authors agree to show that the level has fallen back slightly to − 24 m.

5.1.6. Amplitude and rates of changes

Over the last 2200 years, based on geological data, a conservative amplitude of CSL changes of 8.2 m may be proposed between 1440 AD (core V3A) and 180 AD (core C2), although extremes between the Bagho point and Well 3 horizon in the Kura delta may perhaps suggest that the amplitude could reach a much higher value up to 18 m. Based on archaeo-historical data, a conservative evaluation provides 14.7 m between 1638 AD and two low points at 943–945 AD, and an extreme of 20 m if the highest point in 1306–1320 AD is accepted. Therefore, the investigations over the last 2200 years by including the very low levels in the Late Sasanian period allow highlighting an amplitude of changes much larger that seen by analysing the last millennium only (Naderi Beni et al., 2013), and at least five times larger than that of the last century. This should then feed into mitigation plans for the future.

Although a denser number of data points all along the investigated time interval would be needed to evaluate rate of changes, some periods seem to have been affected by rapid changes. This is the case for three apparent floodings: 1) at the end of the Sasanian period, 2) in 1303–1307 AD and 3) at the beginning of the 17th century. For example, for the relatively well-documented 17th century, the rise of 6.6 m between 1590 AD and 1638 occurred at an average rate of change of 14 cm per year. This is more than during the recent increase: 10.7 cm per year between 1977 and 1995 (Arpe et al., 2020).

5.2. Comparison to other curves

In brief for the period between 1000 and 2200 years ago, our work clearly proposes a pronounced mid-Parthian highstand possibly following a distinct Parthian lowstand, a Late Parthian to mid-Sasanian deep lowstand, a Late Sasanian moderate highstand, and a Medieval period with moderately low levels. Afterwards, the information collated here for the LIA confirms previously published work.

5.2.1. Does the "2600 yr BP highstand" exist?

The Rychagov curve based on uncalibrated dates led him state that CSL did not go higher than −25 m in the last 2500 years (Rychagov, 1977). Although radiocarbon dates are provided in an appendix to his 1977 work, no metadata are available on the precise location and elevation of the samples, nor on the type of material dated, thus making them not sufficiently precise for the purpose of this investigation. In the Turali lagoon, four dates (further to those discussed earlier) are published for the period before 2200 yr BP (Kroonenberg et al., 2007). Their calibration with the new FRO indicates that they are all between 360 and 200 cal BC (median probabilities); moreover none are from sediment at an elevation as high as −24 m (DAG LG HV04; at cal 153 BC-cal 131 AD). Thus the "2600 yr BP highstand" is not represented in the Turali dataset of Kroonenberg et al. (2007). No dates in the work of Varushchenko et al. (1987) cover the "2600 yr BP highstand" as seen by the calibration of dates at points 25 and 22 in his work. Point 25 is at the mouth of the river Ulluchai in Dagestan at −22.7 ± 2 m and 2440 ± 120 ^{14}C BP. When calibrated, it gives an age of 391 cal BC– cal AD171, with a median probability of 109 cal BC, and thus falls in the Parthian highstand. The next older date at a high level (point 22 at −21.5 m in Turali) is at 1160 cal BC (median probability), thus clearly older than a supposed "2600 yr BP highstand". Therefore, the data most commonly used to define this "2600 yr BP highstand" are now in the Parthian highstand and no data exist in Kroonenberg et al. (2007) and Varushchenko et al. (1987) for this period showing a highstand, when the dates are respectively re-calibrated or calibrated. Therefore, this highstand could not be documented here despite in-depth literature search, although it may perhaps otherwise exist.

5.2.2. What of the Derbent regression?

A problem of terminology exists for this period. The name "Derbent regression" or "Derbent lowstand" is generally attributed to the Medieval period but actually seems to refer to two distinct times, both times of lowstands. Some investigations report it at 580–600 AD (Varushchenko et al., 1987; Klige and Myagkov, 1992; Hoogendoorn, 2006;

Kroonenberg et al., 2008) whereas other investigations report it at 1000–1200 AD (Karpychev, 2001; Svitoch, 2012). No stratotype has been defined. The most recent age attribution is the only that justifies calling the Derbent Regression a Medieval regression, as the first one falls in the Sasanian period of Late Antiquity. In some cases, the two lowstands are somewhat blurred together (Rychagov, 1997). It seems however more logical to call the earlier period only the Derbent Regression as this is when the initial wall was built in the Sasanian period, and to avoid using the term Medieval. We recommend thus here to keep away from this appellation or at least call for caution in its usage with clear age precision.

5.2.3. Comparison to the 2013 curve

In comparison to the curve of 2013 (Naderi Beni et al., 2013) starting in the Medieval period, the main difference in the present curve is the much lower water level obtained before 1303–1307 AD. This is mainly due to the rejection of the Brückner date at 915–921 AD based on observations on the Derbent Wall that has probably been reconstructed since, after several earthquakes and coastal subsidence (Brückner, 1890).

5.3. Causes

The precise causes of CSL changes are still being hotly debated: the flow of the Volga River, the current main largest water inflow, being however the dominant driver. The current work makes this topic worth revisiting, because our investigations add precision to the CSL curve especially for the period 200 cal BC to cal 1300 AD.

5.3.1. Potential mechanisms

A preliminary caveat is necessary as the region around the south Caspian Sea is highly **seismic**. For example, the Derbent region of Dagestan (from which many historical and archaeological data are derived) is one of the most actively seismic around the Caspian Sea. In the Derbent area, Bochud (2011) determined a tectonic uplift of 0.46 mm per yr, that would translate into 92 cm over 2000 years. At the foot of the uplifting Alborz Mountain (1 to 5 mm per yr), the coastal plain is subsiding along the Khazar Fault along with the south Caspian basin at a rate of 0.43 mm per yr (Allen et al., 2002; Djamour et al., 2010). At the scale of precision of the data evaluated in our work, the movement is thus considered rather negligible. Ozyavas et al. (2010), analysing CSL from 1998 to 2005 and its water budget, suggested a maximum of 5 cm CSL fall caused by a downward movement of the south Caspian basin, best seen in 2000–2001 after earthquakes in 2000 and 2001. Naderi Beni et al. (2013) also discussed the potential influence of earthquakes and highlight their importance but at a local scale only. Thus, seismicity has only a small impact on elevations at the scale of the last two millennia on average and often only locally.

Additionally, natural hazards (flashfloods or earthquakes) in 1208 AD, 1389, 1405 may have contributed to the natural destruction of dams on the Amu Darya (Boroffka, 2010; Sala, 2019). The Amu Darya flows close to the Bukhara and the Amu Darya Faults where the palaeo Amu Darya splits off from its modern channel, The river is also close to the Ural-Turkestan suture near Urgench. Both areas have known historical and modern tectonic movements (Thomas et al., 1998).

The Syr Darya might have bypassed the Aral Sea and flowed directly in the Amu Darya due to human-made diversions, hence increasing the flow to the Caspian Sea in the early 15th century (Boroffka, 2010; Sala, 2019). In consequence, Khwarasmian river diversions by dam building were frequent between 1221 AD and 1575 (Herzfeld, 1947), but water was reaching the Caspian Sea only until 1417 AD according to Boroffka (2010) (Fig. 8 and 9a). In our reconstruction, it is indeed only at the end of the 15th century that the CSL falls below present-day for ca 100 years before re-increasing.

The Westerlies transport most moisture needed for **precipitation** to the Caspian Sea and over the drainage basin of the currently inflowing

rivers. Stronger Westerlies will bring more precipitation, but will also cause an export of the water vapor further to the east and thus cause a net loss of water for the Caspian drainage basin (Arpe et al., 2020). However, the Summer Indian Monsoon may currently also influence CSL, albeit indirectly. Indeed, meteorological analyses (Schiemann et al., 2007) have shown that a stronger monsoon would warm the air passing over the Pamir - Hindu Kush Mountains where the head waters of the Amu Darya are, causing the melting of glaciers, thus increasing the flow in this important river. In the rare cases when there is river diversion to the CS, then the impact may be felt.

Global **temperature** and summer temperature from tree rings in the Russian Altai both show the Medieval Climatic Anomaly with higher temperatures and the LIA with colder temperatures (Büntgen et al., 2016; PAGES 2k Consortium et al., 2019) (Fig. 9b). In addition, tree ring analysis has highlighted the Late Antique Little Ice Age, LALIA (Büntgen et al., 2016), which was a long-lasting northern hemisphere cooling dated at 536 AD – ~660 (Büntgen et al., 2016) (Fig. 9c), part of the Dark Ages Cold Period at 400–765 AD (Helama et al., 2017) and the warmer temperatures of the Warm Roman period.

In brief, regarding CSL, the balance between precipitation and evaporation is clearly affected by temperature. However as stated before, it will be in the end the loss of water (as vapor) from the CS drainage that will take precedence.

5.3.2. Causes of CSL changes over time

A combination of human and natural causes must be envisaged for an explanation of CSL changes.

The causes of the Late Parthian-Early Sasanian data-poor period (180 AD to 450) could be a very low sea level, leaving on the coast de facto very little traces behind. This low level would have significantly increased the area of the coastal flood plain and free important surfaces newly available to agriculture.

Although the date of the Late Sasanian highstand does not fit the Hun destruction of late 4th century, it is possible that further wars occurred between the Persian Empire, Turkic tribes and Huns in the lower Amu Darya (Oxus) region. Thus further damage to hydraulic infrastructure might have been the reason for the rapid water level increase in the Caspian Sea. This daring hypothesis is triggered by destructions that occurred in the same place but several centuries later. From the climatic point of view the Late Sasanian transgression fits well the LALIA (Fig. 9c). The Late Parthian regression corresponds to the early part of the Warm Roman Period (Fig. 9b and c).

During the Medieval Climate Anomaly, tree-ring analyses in western central Asia indicate that, since 618 AD, the warmest period is between 800 AD and 1000 (Esper et al., 2002), which is also seen in the tree-ring-inferred June–July-August (JJA) temperatures from the Russian Altai (Büntgen et al., 2016) (Fig. 9c). The warmest climatic period seems to have occurred before the expansion of Mongols. The link between climate and CSL is not straightforward as this warm period might have favoured increased evaporation (thus low CSL), although increased precipitations occur during warmer periods as shown in Arpe and Leroy et al. (2007) and Roshan et al. (2012) and lead to an inverse effect on CSL.

The LIA highstand clearly results from multiple causes. The LIA is defined by its colder and wetter climate not only globally, but also in central Asia (references in Putnam et al., 2016) (Fig. 9c). Tree-ring analyses on western central Asia indicate that, since 618 AD, the coldest decades are in 1600–1650 AD, within a longer cold period from 1600 AD to 1800 (Esper et al., 2002). Wetter than current climate in the LIA seems to have favoured Mongol steppe pastoralists and people movements by a southward displacement of grassland (Putnam et al., 2016). The deserts of Kwarazm would have needed to be greener in order to sustain large numbers of horses required by the Mongol army (Putnam et al., 2016). Destruction of irrigation dams by the Mongol invasion at 1221 AD and the Timurid wars at 1372–1388 AD (Sala, 2019) are related to this climatically-driven population movements.

Arpe et al. (2000) highlighted the importance of El-Niño Southern Oscillation (ENSO) for CSL changes. Molavi-Arabshahi et al. (2016) showed a southward shift of the Jet Stream over the Caspian Sea during El Niño events and, with it, a shift of the strong baroclinicity that guides cyclone tracks, bringing more precipitation to the Caspian catchment; thus higher El-Niño events would lead to more precipitation over the Caspian Basin.

In brief it is impossible to assign the various highstands and lowstands to a linear temperature forcing (Fig. 9). Indeed, in one case a cold climate corresponded to a low CSL and in another one to high CSL: clearly the LALIA and the LIA correspond for the former to a lowstand and for the latter one to a highstand. The explanation might perhaps lie with the precipitation that is largely governed by ENSO. It is not yet fully established what the state of ENSO was over the last 2000 years. However, Yan et al. (2011) suggest that it was higher both in the Dark Ages Cold Period and the LIA. Rein et al. (2004) consider as a major anomaly a much weaker el-Niño activity during the Medieval period than during the periods before and after.

The Medieval Climate Anomaly that is warm in central Asia corresponds to relatively low levels (Fig. 9). The Roman Warm Period contains several short-term fluctuations as seen in the tree rings; but the number of CSL points is too low to attach them to any of those short-term climatic fluctuations.

The two extremes in our CSL curve, i.e. the very low levels at 580 AD and the very high levels at 1303–1304 AD (Fig. 9), are both most likely not due to climate only. While the first one has an unknown cause, the second one is most likely owing to a purposeful malignant Amu Darya diversion.

6. Conclusions

In the Caspian Sea, the difficulties of choosing an appropriate radiocarbon calibration scheme and the progress made recently have led to cacophonic and discordant approaches by various authors: no calibration, successive and diverse marine calibrations and successive terrestrial calibrations. This situation has hampered a harmonious combination of information from geology, archaeology, and history. An improved understanding of freshwater reservoir offsets and recalibration of radiocarbon dates with the most recent calibration curve has enabled us to harmonize the timescales of previous datasets where sufficient metadata were available.

Our investigation has highlighted two significant issues when naming well-known lowstands and highstands over of the last >2200 years. Firstly, caution is called when using the term Derbent lowstand, because of the confusing literature. It is thus advised to precisely and clearly state the age and to separate the mid-Sasanian lowstand from the truly Medieval lowstand. Secondly, the evidence used in literature to define the "2600 yr BP highstand" has been revised by calibration or recalibration of the original ^{14}C dates. This revision does not show a highstand at 2600 yr BP (because no data are available at that time, when calibrating the dates) but at a more recent time at ca 50 BC–50 AD termed here the mid-Parthian highstand. Thus again caution should be used, and the name "2600 yr BP highstand" should not be used unless strong, most likely new, data justify it.

A conservative estimation of CSL amplitude change reaches 15 m over the last 2200 years (perhaps even more, i.e. 20 m) with at times high rates of changes calculated as 14 cm per year. Therefore the amplitude is at minimum five times larger than that of the last century, and the rate of change is 25% higher. If such changes were to happen now, our society would have difficulties facing it; it would thus lead to a disaster of likely catastrophic scale. Although we are technologically more advanced, none of the mentioned causes of CSL changes can be avoided nowadays; as indeed a mix of natural hazards, climatic and human causes are invoked to explain the observed CSL changes.

Most interestingly, over the last 2200 years no simple correlation between climate (temperature, precipitation) and sea levels could be found. Although some important changes may be attributed to human interventions (e.g. river diversions), at the larger time scale, climate has to be the main forcing factor. However global temperatures do not seem to be the sole forcing factor, perhaps due to the confounding impact of ENSO and human activities on river diversion.

The current research indicates that further investigations to improve the precision of the Caspian Sea level curve over the last millennia requires well documented radiocarbon ages with a small confidence interval, on well-chosen samples, to be obtained from sites with accurate elevation measurements. Under these conditions only, further insight into water level drivers will come within reach.

Appendix A. Supplementary data

Supplementary data to this article can be found online at https://doi.org/10.1016/j.geomorph.2022.108136.

References

Aliev, A.A., Gadjiev, M.S., Gaither, M.G., Kohl, P.L., Magomedov, R.M., Aliev, I.N., 2006. The Ghilghilchay defensive long wall: new investigations. Ancient West East 5, 143–177.

Allen, M.B., Jones, S., Ismail-Zadeh, A., Simmons, M., Anderson, L., 2002. Onset of subduction as the cause of rapid Pliocene-Quaternary subsidence in the South Caspian basin. Geology 30 (9), 775–778.

Arpe, K., Leroy, S., 2007. The Caspian Sea Level forced by the atmospheric circulation, as observed and modelled. Quat. Int. 173–174, 144–152.

Arpe, K., Bengtsson, L., Golitsyn, S., Mokhov, I.I., Semenov, V.A., Sporyshev, P.V., 2000. Connection between Caspian Sea level variability and ENSO. Geophys. Res. Lett. 27, 2693–2696.

Arpe, K., Tsuang, B.-J., Tseng, Y.-H., Liu, X.-Y., Leroy, S.A.G., 2019. Quantification of climatic feed-backs on the Caspian Sea Level variability and impacts from the Caspian Sea on the large scale atmospheric circulation. Theor. Appl. Climatol. 136 (1–2), 475–488. https://doi.org/10.1007/s00704-018-2481-x.

Arpe, K., Molavi-Arabshahi, M., Leroy, S.A.G., 2020. Wind variability over the Caspian Sea, its impact on Caspian Sea level and the link with ENSO. Int. J. Climatol. https://doi.org/10.1002/joc.6564, 2.

Bates, C.R., Omrani Rekavandi, H., Tofighian, H., 2022. A Bathymetric and Sub-bottom Investigation of the Tammisheh Wall's Northernmost Section Submerged in the Caspian Sea, Chap. 12 in: Sauer et al. 2022.

Bates, C.R., Bates, M., Omrani Rekavandi, H., 2022. Discovering Unknown Sections of the Great Wall of Gorgan Near the Shores of the Caspian Sea, Chap. 11 in: Sauer et al. 2022.

Bennett, K., 2007. psimpoll and pscomb programs for plotting and analysis. http://www.chrono.qub.ac.uk/psimpoll/psimpoll.html (accessed 31 March 2018).

Bezrodnykh, Y.P., Sorokin, V.M., 2016. On the age of the Mangyshlakian deposits of the northern Caspian Sea. Quat. Res. 85 (02), 245–254.

Bochud, M., 2011. Tectonics of the Eastern Greater Caucasus in Azerbaijan. Doctoral thesis 1733, 30. University of Fribourg, Geofocus, 201 pp.

Boroffka, N.G.O., 2010. Archaeology and its relevance to climate and water level changes: a review. In: Kostianoy, A.G., Kosarev, A.N. (Eds.), The Aral Sea Environment. Handbook of Environmental Chemistry, 7, pp. 283–303. https://doi.org/10.1007/698_2009_7.

Brückner, E., 1890. In: Wien, Olmütz, Hölzel, E. (Eds.), Klima-Schwankungen seit 1700: nebst Bemerkungen über die Klimaschwankungen der Diluvialzeit. Bd. 4, Hft. 2.

Büntgen, U., Myglan, V., Ljungqvist, F., et al., 2016. Cooling and societal change during the late Antique Little Ice Age from 536 to around 660 AD. Nat. Geosci. 9, 231–236. https://doi.org/10.1038/ngeo2652.

Djamour, Y., Vernant, P., Bayer, R., Nankali, H., Ritz, J.F., Le Moigne, N., Sedighi, M., Khorrami, F., 2010. GPS and gravity constraints on continental deformation in the Alborz mountain range, Iran. Geophys. J. Int. 183, 1287–1301.

Esper, J., Schweingruber, F.H., Winiger, M., 2002. 1300 years of climatic history for Western Central Asia inferred from tree-rings. The Holocene 12 (3), 267–277.

Gloukhovskoy, A.I., 1893. The Passage of the Water of the Amu-Darya by its Old Bed Into the Caspian Sea. Elibron Classics Replica Edition, St Petersburg.

Haghani, S., Leroy, S.A.G., 2016. Differential impact of long-shore currents on coastal geomorphology development in the context of rapid sea level changes: the case of the Old Sefidrud (Caspian Sea). Quat. Int. 408, 78–92.

Haghani, S., Leroy, S.A.G., Wesselingh, F.P., Rose, N.L., 2016. Rapid evolution of a Ramsar site in response to human interference under rapid sea level change: a South Caspian Sea case study. Quat. Int. 408, 93–112.

Heaton, T., et al., 2020. Marine20—the marine radiocarbon age calibration curve (0–55,000 cal BP). Radiocarbon 62 (4), 779–820.

Helama, S., Jones, P.D., Briffa, K.R., 2017. Dark Ages Cold Period: a literature review and directions for future research. The Holocene 27 (10), 1600–1606.

Herzfeld, E., 1947. In: Zoroaster and His World, 2. Princeton University Press, pp. 411–851.

Hoogendoorn, R.M., 2006. The Impact of Changes in Sediment Supply and Sea-level on Fluvio-deltaic Stratigraphy. Doctoral thesis. Delft University of Technology, 159 pp.

Hoogendoorn, R.M., Boels, J.F., Kroonenberg, S.B., Simmons, M.D., Aliyeva, E., Babazadeh, A.D., Huseynov, D., 2005. Development of the Kura delta, Azerbaijan; a record of Holocene Caspian Sea-level changes. Mar. Geol. 222–223, 359–380.

Hoogendoorn, R.M., Levchenko, O., Missiaen, T., Lychagin, M., Richards, K., Gorbunov, A., Kasimov, N., Kroonenberg, S.B., 2010. High resolution seismic stratigraphy of the modern Volga delta, Russia. In: Proceedings of the International Conference, The Caspian Region, Moscow, pp. 32–37.

Hoyle, T., Leroy, S.A.G., López-Merino, L., van Baak, C., Martinez Cortizas, A., Richards, K., Aghayeva, V., 2021. Biological turnovers in response to marine incursion into the Caspian Sea at the Plio-Pleistocene transition. Glob. Planet. Chang. 206, 103623.

Hydroweb, 2021. Lake Caspian. http://hydroweb.theia-land.fr/hydroweb/view/L_caspian?lang=en (accessed 27 August 2021).

Kakroodi, A.A., Kroonenberg, S.B., Hoogendoorn, R.M., Mohammadkhani, H., Yamani, M., Ghassemi, M.R., Lahijani, H.A.K., 2012. Rapid Holocene Sea-level changes along the Iranian Caspian coast. Quat. Int. 263, 93–103.

Kakroodi, A.A., Kroonenberg, S.B., Goorabi, A., Yamani, M., 2014a. Shoreline Response to Rapid 20th Century Sea-Level change along the Iranian Caspian coast. J. Coast. Res. 30 (6), 1243–1250.

Kakroodi, A.A., Kroonenberg, S.B., Naderi Beni, A., Noehgar, N., 2014. Short- and long-term development of the Miankaleh Spit, Southeast Caspian Sea, Iran. J. Coast. Res. 30 (6), 1236–1242.

Kakroodi, A.A., Leroy, S.A.G., Kroonenberg, S.B., Lahijani, H.A.K., Alimohammadian, H., Boomer, I., Goorabi, A., 2015. Late Pleistocene and Holocene Sea-level change and coastal palaeoenvironment along the Iranian Caspian shore. Mar. Geol. 361, 111–125.

Karpychev, Y.A., 1993. Reconstruction of Caspian Sea level fluctuations: radiocarbon dating coastal and bottom deposits. Radiocarbon 35, 409–420.

Karpychev, Y.A., 1998. Dating of regressive stages in the Caspian Sea using 14C. Vodn. Resur. 25, 274–278 (In Russian).

Karpychev, Y.A., 2001. Variation in the Caspian Sea level in the Historic Epoch. Water Resour. 1, 1–14.

Klige, R.K., Myagkov, M.S., 1992. Changes in the water regime of the Caspian Sea. GeoJournal 27 (3), 299–307.

Koriche, S.A., Nandini-Weiss, S.D., Prange, M., Singarayer, J.S., Arpe, K., Cloke, H.L., Schulz, M., Bakker, P., Leroy, S.A.G., Coe, M., 2021. Impacts of variations in Caspian Sea surface area on catchment-scale and large-scale climate. JGR-Atmosphere. https://doi.org/10.1029/2020JD034251.

Kouraev, A.V., Crétaux, J.-F., Lebedev, S.A., Kostianoy, A.G., Ginzburg, A.I., Sheremet, N. A., Mamedov, R., Zhakharova, E.A., Roblou, L., Lyard, F., Calmant, S., Bergé-Nguyen, M., 2011. The Caspian Sea. In: Vignudelli, S., Kostianoy, A.G., Cipollini, P., Benveniste, J. (Eds.), Handbook on Coastal Altimetry, 19. Springer, pp. 331–366. Bd. 4, Hft. 2.

Krivonogov, K.S., Burr, G.S., Kuzmin, Y.V., Gusskov, S.A., Kurmanbaev, R.K., Kenshinbay, T.I., Voyakin, D.A., 2014. The fluctuating Aral Sea: a multidisciplinary-based history of the last two thousand years. Gondwana Res. 26, 284–300.

Kroonenberg, S.B., Abdurakhmanov, G.M., Badyukova, E.N., van der Borg, K., Kalashnikov, A., Kasimov, N., Rychagov, G.I., Svitoch, A.A., Vonhof, H.B., Wesselingh, F.P., 2007. Solar-forced 2600 BP and Little Ice Age highstands of the Caspian Sea. Quat. Int. 173–174, 137–143.

Kroonenberg, S.B., Kasimov, N.S., Lychagin, M.Yu., 2008. The Caspian Sea, a natural laboratory for sea-level change. Geogr. Environ. Sustain. 1 (1), 22–37.

Kudrjavcev, A.A., Gadžiev, M.S., 2002. In: Archäologische Unterwasseruntersuchungen an der Küste von Darband. Archäologische Mitteilungen aus Iran, 33, for 2001, pp. 333–356.

Kurtubadze, M., 2020. Population by number in the Caspian Sea region per cities and administrative units. https://www.grida.no/resources/13601. Accessed 11 Septembre 2021.

Kuzmin, Y., Nevesskaya, L., Krivonogov, S., Burr, G., 2007. Apparent 14 C ages of the 'pre-bomb' shells and correction values (R, ΔR) for Caspian and Aral Seas (Central Asia). Nucl. Instrum. Methods Phys. Res., Sect. B 259, 463–466.

Lahijani, H., Rahimpour-Bonab, H., Tavakoli, V., Hosseindoost, M., 2009. Evidence for late Holocene highstands in Central Guilan - East Mazandaran, South Caspian coast, Iran. Quat. Int. 197, 55–71.

Leroy, S.A.G., Marret, F., Gibert, E., Chalié, F., Reyss, J.-L., Arpe, K., 2007. River inflow and salinity changes in the Caspian Sea during the last 5500 years. Quat. Sci. Rev. 26, 3359–3383.

Leroy, S.A.G., Lahijani, H.A.K., Djamali, M., Naqinezhad, A., Moghadam, M.V., Arpe, K., Shah-Hosseini, M., Hosseindoust, M., Miller, C.S., Tavakoli, V., Habibi, P., Naderi Beni, M., 2011. Late Little Ice Age palaeoenvironmental records from the Anzali and Amirkola lagoons (south Caspian Sea): vegetation and sea level changes. Palaeogeogr. Palaeoclimatol. Palaeoecol. 302, 415–434.

Leroy, S.A.G., Kakroodi, A.A., Kroonenberg, S.B., Lahijani, H.A.K., Alimohammadian, H., Nigarov, A., 2013a. Holocene vegetation history and sea level changes in the SE corner of the Caspian Sea: relevance to SW Asia climate. Quat. Sci. Rev. 70, 28–47.

Leroy, S.A.G., Lahijani, H.A.K., Reyss, J.-L., Chalié, F., Haghani, S., Shah-Hosseini, M., Shahkarami, S., Tudryn, A., Arpe, K., Habibi, P., Nasrollahzadeh, H.S., Makhlough, A., 2013b. A two-step expansion of the dinocyst Lingulodinium machaerophorum in the Caspian Sea: the role of changing environment. Quat. Sci. Rev. 77, 31–45.

Leroy, S.A.G., Chalié, F., Wesselingh, F., Sanjani, S., Lahijani, H.A.K., Athersuch, J., Struck, U., Plunkett, G., Reimer, P.J., Habibi, P., Kabiri, K., Haghani, S., Naderi Beni, A., Arpe, K., 2018. Multiproxy indicators in a Pontocaspian system: a depth transect of surface sediment in the S-E Caspian Sea. Geol. Belg. 21 (3-4), 143–165.

Leroy, S.A.G., López-Merino, L., Kozina, N., 2019. Caspian deep-water dinocyst records show a reversed meridional water gradient at 8.5 – 4.0 cal. ka BP. Quat. Sci. Rev. 209, 1–12. https://doi.org/10.1016/j.quascirev.2019.02.011 and supplem information.

Leroy, S.A.G., Amini, A., Gregg, M., Marinova, E., Bendrey, R., Zha, Y., Naderi Beni, A. M., Fazeli Nashli, H., 2019. Human responses to environmental changes on the southern coastal plain of the Caspian Sea during the Mesolithic and Neolithic periods. Quat. Sci. Rev. 218, 343–364 and supplementary information.

Leroy, S.A.G., Lahijani, H., Crétaux, J.-F., Aladin, N., Plotnikov, I., 2020. Past and current changes in the largest lake of the world: the Caspian Sea. In: Mischke, S. (Ed.), Large Asian Lakes in a Changing World. Springer. https://doi.org/10.1007/978-3-030-42254-7. ISBN 978-3-030-42253-0.

Leroy, S.A.G., Demory, F., Chalié, F., Bates, R., Bates, M., Omrani Rekavandi, H., Sauer, E., 2022. In: Sauer, E. (Ed.), Palaeoenvironments at the Caspian Terminals of the Gorgan and Tammisheh Walls, Chap. 13, 2022.

Létolle, R., 2000. Histoire de l'Ouzboï, cours fossile de l'Amou Daria: synthèse et éléments nouveaux. Stud. Iran. 29, 195–240.

Létolle, R., Mainguet, M., 1993. Aral. Springer-Verlag, Paris, 357 pp.

Maksaev, K.K., Svitoch, A.A., Yanina, T.A., Badyukova, E.N., Khomchenko, D.S., Oshchepkov, G.V., 2015. Lower Khvalynian sediment record on the Middle and Lower Volga region. In: IGCP 610 Third Plenary Conference and Field Trip, Astrakhan, Russia, 22-30 September, 2015, pp. 126–128.

Mann, M.E., 2002. Little Ice Age. In: MacCracken, M., Perry, J.S. (Eds.), Encyclopedia of Global Environmental Change. J. Wiley and Sons Ltd, Chichester, pp. 504–509.

Mann, M.E., Bradley, R.S., Hughes, M.K., 2009. Global-scale temperature patterns and climate forcing over the past six centuries. Nature 392, 779–788.

Marriner, N., Morhange, C., 2006. Geoarchaeological evidence for dredging in Tyre's ancient harbour. Levant. Quat. Res. 65, 164–171.

McCarthy, F.M.G., Mudie, P.J., 1998. Oceanic pollen transport and pollen: dinocyst ratios as markers of late Cenozoic Sea level change and sediment transport. Palaeogeogr. Palaeoclimatol. Palaeoecol. 138, 187–206.

Mertens, K.N., Ribeiro, S., Bouimetarhan, I., Caner, H., Combourieu-Nebout, N., Dale, B., de Vernal, A., Ellegaard, M., Filipova, M., Godhe, A., Goubert, E., Grøsfjeld, K., Holzwarth, U., Kotthoff, U., Leroy, S.A.G., Londeix, L., Marret, F., Matsuoka, K., Mudie, P.J., Naudts, L., Peña-Manjarrez, J.L., Persson, A., Popescu, S.-M., Pospelova, V., Sangiorgi, F., van der Meer, M., Vink, A., Zonneveld, K.A.F., Vercauteren, D., Vlassenbroeck, J., Louwye, S., 2009. Process length variation in cysts of a dinoflagellate, Lingulodinium machaerophorum, in surface sediments: investigating its potential as salinity proxy. Mar. Micropaleontol. 70 (1–2), 54–69.

Mertens, K.N., Bradley, L.R., Takano, Y., Mudie, P.J., Marret, F., Aksu, A.E., Hiscott, R.N., Verleye, T.J., Mousing, E.A., Smyrnova, L.L., Bagheri, S., Mansor, M., Pospelova, V., Matsuoka, K., 2012. Quantitative estimation of Holocene surface salinity variation in the Black Sea using dinoflagellate cyst process length. Quat. Sci. Rev. 39, 45–59.

Molavi-Arabshahi, M., Arpe, K., Leroy, S.A.G., 2016. Precipitation and temperature of the Southwest Caspian Sea during the last 55 years, their trends and teleconnections with large-scale atmospheric phenomena. Int. J. Climatol. 36, 2156–2172.

Mudie, P., Marret, F., Mertens, K., Shumilovikikh, L., Leroy, S.A.G., 2017. Atlas of modern dinoflagellate cyst distributions in the Black Sea Corridor, including Caspian and Aral Seas. Mar. Micropaleontol. 134, 1–152. https://doi.org/10.1016/j.marmicro.2017.05.004.

Naderi Beni, A., Lahijani, H., Mousavi Harami, R., Arpe, K., Leroy, S.A.G., Marriner, N., Berberian, M., Andrieu-Ponel, V., Djamali, M., Mahboubi, A., Reimer, P.J., 2013. Caspian Sea level changes during the last millennium: historical and geological evidences from the South Caspian Sea. Clim. Past 9, 1645–1665.

Naderi Beni, A., Lahijani, H., Pourkerman, M., Jokar, R., Djamali, M., Marriner, N., Andrieu-Ponel, V., Mousavi, H., 2014. Late Holocene Caspian Sea level changes and its impacts on low lying coastal evolution: a multidisciplinary case study from south Southeastern flank of the Caspian Sea. J. Pers. Gulf (Marine Science) 5 (22), 27–48.

Nadim, M., Zahedi, G., 2018. Qozloq route (Astrabad to Shahrud) impact on economic developments of the region (Safavid Course). J. Polit. Law 11 (2), 6–15.

Nokandeh, J., Sauer, E.W., Omrani Rekavandi, H., Wilkinson, T., Abbasi, G.A., Schwenninger, J.-L., Mahmoudi, M., Parker, D., Fattahi, M., Usher-Wilson, L.S., Ershadi, M., Ratcliffe, J., Gale, R., 2006. Linear barriers of Northern Iran: the Great Wall of Gorgan and the Wall of Tammishe. Iran 44, 121–173.

Ollivier, V., Fontugne, M., Lyonnet, B., Chataigner, C., 2016. Base level changes, river avulsions and Holocene human settlement dynamics in the Caspian Sea area (middle Kura valley, South Caucasus). Quat. Int. 395, 79–94.

Olsson, I.U., 1980. Content of 14C in marine mammals from northern Europe. Radiocarbon 22, 662–675.

Ozyavas, A., Shuhab, D.K., Casey, J.F., 2010. A possible connection of Caspian Sea level fluctuations with meteorological factors and seismicity. Earth Planet. Sci. Lett. 299, 150–158.

PAGES 2k Consortium, Neukom, R., Barboza, L.A., 2019. Consistent multidecadal variability in global temperature reconstructions and simulations over the Common Era. Nat. Geosci. 12, 643–649. https://doi.org/10.1038/s41561-019-0400-0.

Putnam, A.E., Putnam, D., Andreu-Hayles, L., Cook, E.R., Palmer, J.G., Clark, E.H., Wang, C., Chen, F., Denton, G., Boyle, D.P., Bassett, S., Birkel, S.D., Martin Fernandez, J., Hajdas, I., Southon, J.R., Garner, C., Broecker, W.S., 2016. Little Ice Age wetting of interior asian deserts and the rise of the Mongol Empire. Quat. Sci. Rev. 131, 33–50.

Ramezani, E., Mrotzek, A., Mohadjer, M., Kakroodi, A.A., Kroonenberg, S.B., Joosten, H., 2016. Between the mountains and the sea: Late-Holocene Caspian Sea level fluctuations and vegetation history of the lowland forests of northern Iran. Quat. Int. 408, 52–64.

Reimer, P.J., Austin, W.E.N., Bard, E., Bayliss, A., Blackwell, P.G., Bronk Ramsey, C., Butzin, M., Cheng, H., Edwards, R.L., Friedrich, M., Grootes, P.M., Guilderson, T.P., Hajdas, I., Heaton, T.J., Hogg, A.G., Hughen, K.A., Kromer, B., Manning, S.W., Muscheler, R., Palmer, J.G., Pearson, C., Van Der Plicht, J., Reimer, R.W., Richards, D.A., Scott, E.M., Southon, J.R., Turney, C.S.M., Wacker, L., Adolphi, F., Büntgen, U., Capano, M., Fahrni, S.M., Fogtmann-Schulz, A., Friedrich, R., Köhler, P., Kudsk, S., Miyake, F., Olsen, J., Reinig, F., Sakamoto, M., Sookdeo, A., Talamo, S., 2020. The IntCal20 Northern Hemisphere radiocarbon age calibration Curve (0–55 cal kBP). Radiocarbon 62, 725–757.

Rein, B., Lückge, A., Sirocko, F., 2004. A major Holocene ENSO anomaly during the medieval period. Geophys. Res. Lett. 31, L17211 https://doi.org/10.1029/2004GL020161.

Rekavandi, 2007. An imperial frontier of the Sasanian Empire: further fieldwork at the great wall of Gorgan. Iran 45 (1), 95–136.

Roshan, G.R., Masumeh Moghbel, M., Grab, S., 2012. Modelling Caspian Sea water level oscillations under different scenarios of increasing atmospheric carbon dioxide concentrations. Iran. J. Environ. Health Sci. Eng. 9, 24.

Rychagov, G.I., 1977. Abstract, DSc Thesis, Moscow. In: Pleistocenovaya istorija Kaspiiskogo morya, p. 62 (In Russian).

Rychagov, G.I., 1997. Holocene oscillations of the Caspian Sea, and forecasts based on palaeogeographical reconstructions. Quat. Int. 41 (42), 167–172.

Sala, R., 2019. Quantitative evaluation of the impact on Aral Sea levels by anthropogenic water withdrawal and Syr Darya course diversion during the Medieval period (1.0–0.8 ka BP). In: Yang, L.E., Bork, H.-R., Fang, X., Mischke, S. (Eds.), Socio-environmental Dynamics Along the Historical Silk Road. Springer Nature Switzerland, pp. 95–122.

Sauer, E.W., Omrani Rekavandi, H., Wilkinson, T.J., Nokandeh, J., Hopper, K., Abbasi, G. A., Ainslie, R., Roustaei, K., MacDonald, E., Safari Tamak, E., Ratcliffe, J., Mahmoudi, M., Oatley, C., Ershadi, M., Usher-Wilson, L.S., Nazifi, A., Griffiths, S., Shabani, B., Parker, D., Mousavi, M., Galiatsatos, N., Tolouei, H., Mashkour, M., Batt, C.M., Greenwood, D.P., Jansen Van Rensburg, J., Caputo, F., Radu, V., Schwenninger, J.-L., Fattahi, M., Gale, R., Poole, I., Hoffmann, B., Evershed, R., Thomas, R., with contributions by Priestman S., 2013. Persia's Imperial Power in Late Antiquity: The Great Wall of Gorgan and Frontier Landscapes of Sasanian Iran. A Joint Fieldwork Project by the Iranian Cultural Heritage, Handcraft and Tourism Organisation, the Iranian Center for Archaeological Research and the Universities of Edinburgh and Durham (2005–2009). In: British Institute of Persian Studies Archaeological Monographs Series, II, Oxford. ISBN 978-1-84217-519-4.

Sauer, E.W., Nokandeh, J., Omrani Rekavandi, H., 2022. Ancient arms race: Antiquity's largest fortresses and Sasanian military networks of Northern Iran. In: A Joint Fieldwork Project by the Iranian Center for Archaeological Research, the Research Institute of Cultural Heritage and Tourism and the University of Edinburgh (2014–2016). British Institute of Persian Studies Archaeological Monographs Series, VII, Oxford (accessed 27 August 2021).

Schiemann, R., Glazirina, M.G., Schär, C., 2007. On the relationship between the Indian summer monsoon and river flow in the Aral Sea basin. Geophys. Res. Lett. 34 (5), L05706.

Stuiver, M., Quay, P.D., 1981. Atmospheric C-14 changes resulting from fossil-fuel CO2 release and cosmic-ray flux variability. Earth Planet. Sci. Lett. 53, 349–362.

Stuiver, M., Reimer, P.J., Reimer, R.W., 2021. CALIB 8.2 [WWW program]. at. http://calib.org (accessed 9 March 2021).

Svitoch, A.A., 2012. The Caspian Sea shelf during the Pleistocene regressive epochs. Oceanology 52 (4), 526–539.

Thomas, J.-C., Grasso, J.-R., Bossu, R., Martinod, J., Nurtaev, B., 1998. Recent deformation in the Turan and south Kazakh platforms, western Central Asia in relation to Arabia-Asia and India-Asia collisions. Tectonics 18 (2), 201–214.

Thorley, J., 1969. In: The Development of Trade Between the Roman Empire and the East under Augustus. Greece & Rome, Second Series, 16, pp. 209–223, 2.

Toonen, W.H.J., Macklin, M.G., Dawkes, G., Durcan, J.A., Leman, M., Nikolayev, Y., Yegorov, A., 2020. A hydromorphic reevaluation of the forgotten river civilizations of Central Asia. PNAS 117 (52), 32982–32988 www.pnas.org/cgi/doi/.

Van de Velde, S., Yanina, T.A., Neubauer, T., Wesselingh, F.P., 2020. The late Pleistocene mollusk fauna of Selitrennoye (Astrakhan province, Russia): a natural baseline for endemic Caspian Sea faunas. J. Great Lakes Res. 46 (5), 1227–1239.

Varushchenko, S., Varushchenko, A., Klige, R., 1987. Changes in the Regime of the Caspian Sea and Closed Basins in Time. Nauka, Moscow (in Russian).

Yan, H., Sun, L., Huang, W., Qiu, S., Yang, C., 2011. A record of the Southern Oscillation Index for the past 2,000 years from precipitation proxies. Nat. Geosci. https://doi.org/10.1038/ngeo1231.

Zonn, I., Kostianoy, A., Kosarev, A., Glantz, M., 2010. The Caspian Sea Encyclopedia. Springer, Berlin-Heidelberg, 525 pp.